Article

Cell Host & Microbe

An epithelial-immune circuit amplifies inflammasome and IL-6 responses to SARS-CoV-2

Graphical abstract

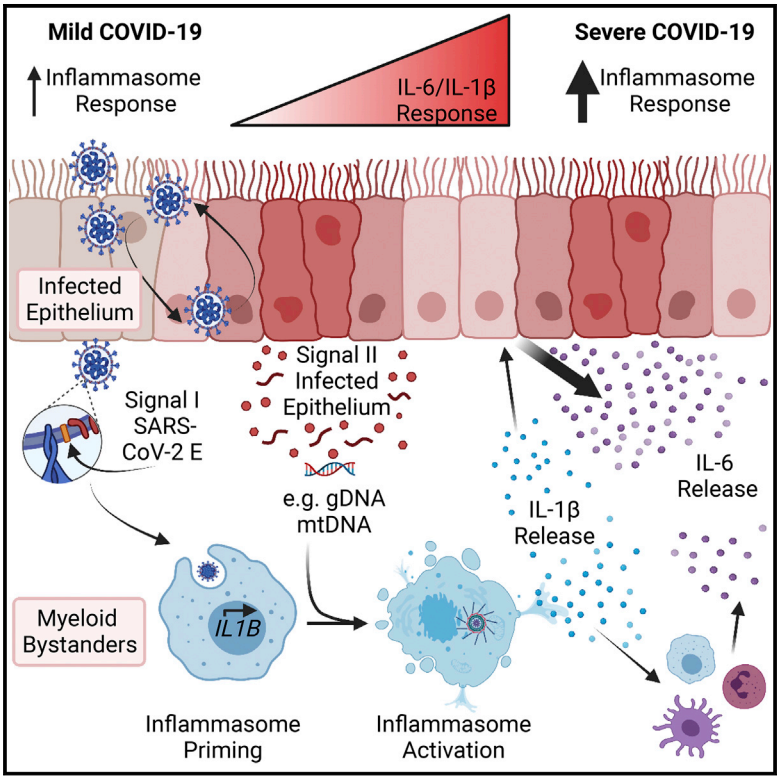

Highlights

- SARS-CoV-2-infected epithelial cells stimulate IL-1β secretion in co-cultured PBMCs
- SARS-CoV-2 E protein primes and DNA DAMPs activate inflammasomes in leukocytes
- IL-1β stimulates IL-6 secretion from epithelial and immune cells
- Intensified inflammasome priming is observed in BALF from severe COVID-19 patients

Authors

Katherine C. Barnett, Yuying Xie, Takanori Asakura, ..., Yu Leo Lei, Richard C. Boucher, Jenny P.-Y. Ting

Correspondence

jenny_ting@med.unc.edu

In brief

IL-1β and IL-6 are increased in severe COVID-19. Examining the underlying mechanisms, Barnett et al. show that SARS-CoV-2 E protein primes, and DNA from infected epithelial cells activates, inflammasome-dependent IL-1β secretion from leukocytes, which in turn stimulates IL-6 release from epithelial cells.

Barnett et al., 2023, Cell Host & Microbe *31*, 1–17
February 8, 2023
https://doi.org/10.1016/j.chom.2022.12.005

CellPress

Please cite this article in press as: Barnett et al., An epithelial-immune circuit amplifies inflammasome and IL-6 responses to SARS-CoV-2, Cell Host & Microbe (2022), https://doi.org/10.1016/j.chom.2022.12.005

Cell Host & Microbe

CellPress

Article

An epithelial-immune circuit amplifies inflammasome and IL-6 responses to SARS-CoV-2

Katherine C. Barnett,[1,2,3,11] Yuying Xie,[4,5,11] Takanori Asakura,[6,11] Dingka Song,[1,2,3,13] Kaixin Liang,[1,2,3,7] Sharon A. Taft-Benz,[1] Haitao Guo,[1,2,3] Shuangshuang Yang,[1,2,3] Kenichi Okuda,[6] Rodney C. Gilmore,[6] Jennifer F. Loome,[3] Thomas H. Oguin III,[8] Gregory D. Sempowski,[8,14] Scott H. Randell,[5] Mark T. Heise,[1,3] Yu Leo Lei,[9,10,12] Richard C. Boucher,[6,12] and Jenny P.-Y. Ting[1,2,3,12,15,*]

[1]Department of Genetics, University of North Carolina at Chapel Hill, Chapel Hill, NC 27599, USA
[2]Lineberger Comprehensive Cancer Center, University of North Carolina at Chapel Hill, Chapel Hill, NC 27599, USA
[3]Department of Microbiology and Immunology, University of North Carolina at Chapel Hill, Chapel Hill, NC 27599, USA
[4]Department of Computational Mathematics, Science and Engineering, Michigan State University, East Lansing, MI 48824, USA
[5]Department of Statistics and Probability, Michigan State University, East Lansing, MI 48824, USA
[6]Marsico Lung Institute, University of North Carolina at Chapel Hill, Chapel Hill, NC 27599, USA
[7]Oral and Craniofacial Biomedicine Program, Adams School of Dentistry, University of North Carolina at Chapel Hill, Chapel Hill, NC 27599, USA
[8]Duke Human Vaccine Institute, Durham, NC 27701, USA
[9]Department of Periodontics and Oral Medicine, Rogel Cancer Center, University of Michigan, Ann Arbor, MI 48104, USA
[10]Department of Otolaryngology-Head and Neck Surgery, Rogel Cancer Center, University of Michigan, Ann Arbor, MI 48109, USA
[11]These authors contributed equally
[12]Senior author
[13]Present address: State Key Laboratory of Oncogenes and Related Genes, Center for Single-Cell Omics, School of Public Health, Shanghai Jiao Tong University School of Medicine, Shanghai 200025, China
[14]Present address: RTI International, Research Triangle Park, Durham, NC 27709, USA
[15]Lead contact
*Correspondence: jenny_ting@med.unc.edu
https://doi.org/10.1016/j.chom.2022.12.005

SUMMARY

Elevated levels of cytokines IL-1β and IL-6 are associated with severe COVID-19. Investigating the underlying mechanisms, we find that while primary human airway epithelia (HAE) have functional inflammasomes and support SARS-CoV-2 replication, they are not the source of IL-1β released upon infection. In leukocytes, the SARS-CoV-2 E protein upregulates inflammasome gene transcription via TLR2 to prime, but not activate, inflammasomes. SARS-CoV-2-infected HAE supply a second signal, which includes genomic and mitochondrial DNA, to stimulate leukocyte IL-1β release. Nuclease treatment, STING, and caspase-1 inhibition but not NLRP3 inhibition blocked leukocyte IL-1β release. After release, IL-1β stimulates IL-6 secretion from HAE. Therefore, infection alone does not increase IL-1β secretion by either cell type. Rather, bi-directional interactions between the SARS-CoV-2-infected epithelium and immune bystanders stimulates both IL-1β and IL-6, creating a pro-inflammatory cytokine circuit. Consistent with these observations, patient autopsy lungs show elevated myeloid inflammasome gene signatures in severe COVID-19.

INTRODUCTION

The emergence of SARS-CoV-2 caused the COVID-19 pandemic that continues to cause global economic disruption, morbidity, and mortality. COVID-19 presentations vary widely, ranging from asymptomatic to fatal disease. Patient characteristics, including age and underlying medical conditions, increase the risk for severe COVID-19,[1] a disease that reflects significant immune dysfunction[2–4] and can lead to fatalities through a hyperinflammatory cytokine storm.[5,6] Severe COVID-19 is associated with high levels of pro-inflammatory cytokines[7,8] and an influx of blood-derived myeloid populations into the lung.[9,10] Recent clinical trial data underscore the relevance of interleukin (IL)-1 and IL-6 in severe COVID-19 because treatment with either IL-1 or IL-6 receptor antagonists increases patient survival and decreases the duration of hospital and intensive care unit stays.[11–13] Therefore, identifying how SARS-CoV-2 stimulates these cytokines is essential to understanding and treating severe COVID-19.

One source of IL-1 in COVID-19 is activation of the inflammasome, an innate immune sensory machinery that initiates IL-1β and IL-18 secretion and pyroptotic cell death.[14] IL-1β, IL-18, and lactate dehydrogenase (LDH), a protein released from pyroptotic cells, are increased in severe COVID-19 patients.[15,16]

Please cite this article in press as: Barnett et al., An epithelial-immune circuit amplifies inflammasome and IL-6 responses to SARS-CoV-2, Cell Host & Microbe (2022), https://doi.org/10.1016/j.chom.2022.12.005

These cytokines may also contribute to COVID-19-associated neurological symptoms.[17,18] While some suggested targeting the inflammasome in severe COVID-19,[19] this pathway may have a protective role, as its loss increases morality to other respiratory viruses.[20–22] Such a contrast in potential functions warrants investigation of how the inflammasome is activated by SARS-CoV-2 and how its activity is altered between COVID-19 disease states.

Many viruses induce inflammasome formation,[23] a two-step process. A signal I, typically provided by Toll-like receptor (TLR) agonists or cytokines, primes a cell for inflammasome activation by upregulating inflammasome-related genes and inducing post-translational modifications to component proteins.[24] During infection, viral nucleic acids or surface proteins may activate TLRs to supply this signal I.[25,26] Then, a cytosolic signal II nucleates the inflammasome through activation of one of many sensors, including nucleotide-binding leucine-rich-repeat (NLR) family pyrin-domain-containing 3 (NLRP3), and absent in melanoma 2 (AIM2).[14] Activated inflammasome sensors interact with the adaptor protein apoptosis-associated speck-like protein containing a caspase activation and recruitment domain (CARD) (ASC) and caspase-1 to form the canonical inflammasome. Then, caspase-1 mediates maturation and secretion of IL-1β and IL-18 and processing of gasdermin D (GSDMD) to form a plasma membrane pore, facilitating pyroptotic cell death.[27–30]

Inflammasome activation occurs in the cytosol, therefore whether a virus acts as a signal II depends on its ability to enter the responding cell and replicate. Some viruses, like influenza A virus (IAV), infect a wide range of cell types, including myeloid cells enriched in inflammasome pathway expression,[31] and indeed, IAV replication activates the NLRP3 inflammasome in myeloid cells.[20–22] SARS-CoV-2, however, requires angiotensin converting enzyme 2 (ACE2) for entry,[32,33] limiting its cellular tropism. Because myeloid cells do not express ACE2,[34–36] inflammasome activation by SARS-CoV-2 replication may be limited to ACE2+ cell types or infection may activate the inflammasome indirectly with damage-associated molecular patterns (DAMPs) generated as a by-product of viral replication acting as an inflammasome-nucleating signal II.

Several studies addressed a third possibility, in which SARS-CoV-2 replication directly activates the inflammasome in monocytes despite these hindrances.[37–41] Reported mechanisms by which SARS-CoV-2 activates the inflammasome vary between studies as does the mechanism of viral entry and replication. One group suggests SARS-CoV-2 is a signal II, requiring an exogenous signal I,[38] while another suggests the SARS-CoV-2 spike (S) protein primes inflammasomes, requiring an exogenous signal II.[39] Yet, another report indicated SARS-CoV-2 enters monocytes upon addition of anti-SARS-CoV-2 antibodies through Fc receptor ɣ, initiating inflammasome activation through abortive replication. Monocyte entry and inflammasome activation was limited to a small percentage of cells in culture and not observed with antibodies from vaccinated patients or healthy individuals.[40] Two other studies suggest SARS-CoV-2 is both signals I and II in myeloid cells. One did not describe a viral entry mechanism,[37] while another reported ACE2 on human lung macrophages mediates viral entry,[41] an observation contrasting the findings of several other groups.[34–36] The conflicting nature of these reports mandates further investigation. Though previous work focused on SARS-CoV-2 infection in monocytes, viral replication occurs predominantly in the airway and nasal epithelium,[42] and one group suggests viral protease activity both activates and inhibits inflammasomes in the airway epithelium.[43] However, to date, no studies have addressed contributions of the epithelium in concert with immune cells to generate an inflammatory milieu, despite enhanced immune-epithelial interactions in severe COVID-19.[44]

Here, we report primary human airway epithelia (HAE) have functional inflammasomes, support SARS-CoV-2 replication but do not release IL-1β during infection. Instead, myeloid bystanders secrete IL-1β in the presence of infected epithelial cells. The envelope (E) protein on the virion surface primes myeloid cells for inflammasome activation. The infected epithelium releases double-stranded DNA (dsDNA), a well-characterized inflammasome agonist,[45–47] supplying signal II. Co-culture of primary human leukocytes with SARS-CoV-2-infected cells, but not each cell type in isolation, stimulates IL-1β release. Thus, interactions between the infected epithelium and leukocytes are required for IL-1β production in COVID-19. Supporting these findings, COVID-19 autopsy lungs revealed inflammasome priming and activation in myeloid cells lacking SARS-CoV-2 antigens. Additionally, meta-analysis of bronchioalveolar lavage fluid (BALF) scRNA-seq data revealed that severe COVID-19 patients have high variation in inflammasome gene expression, suggesting loss of regulation of inflammasome priming. These *in vivo* data corroborate an indirect model of inflammasome activation in COVID-19 and show divergence of inflammasome responses in different COVID-19 patients. Epithelial-immune communication is not limited to inflammasome activation. IL-1β promoted IL-6 release from human leukocytes and HAE, where HAE showed strikingly higher IL-6 production than peripheral blood mononuclear cells (PBMCs). Co-culture of HAE and PBMC during infection promoted IL-1β and IL-1-dependent IL-6 release. Thus, we find that infected epithelial cells drive inflammasome activation in myeloid bystander cells to secrete IL-1β, which in turn promotes IL-6 release from both cell types, creating a pro-inflammatory circuit in COVID-19.

RESULTS

HAE can activate inflammasome-mediated IL-1β release but do not in response to SARS-CoV-2 infection

We first evaluated inflammasome activation by SARS-CoV-2 infection in ACE2+ epithelial cells. Because SARS-CoV-2 infection is species specific and immortalized cell lines often lack innate immune sensors,[48] we utilized well-differentiated, primary HAE grown at an air-liquid interface (ALI), a culture system that recapitulates the pseudostratified epithelium of human airways.[49] Previous work demonstrated SARS-CoV-2 replication in the ciliated cells of these cultures,[42] making them an ideal model to study the intracellular innate immune response to SARS-CoV-2 infection.

While inflammasomes are characterized thoroughly in myeloid cells, mechanisms of inflammasome activation in the human airway epithelium are not well understood. To characterize inflammasomes in HAE, we exposed these cultures to multiple priming and activation stimuli and assessed IL-1β

Please cite this article in press as: Barnett et al., An epithelial-immune circuit amplifies inflammasome and IL-6 responses to SARS-CoV-2, Cell Host & Microbe (2022), https://doi.org/10.1016/j.chom.2022.12.005

CellPress

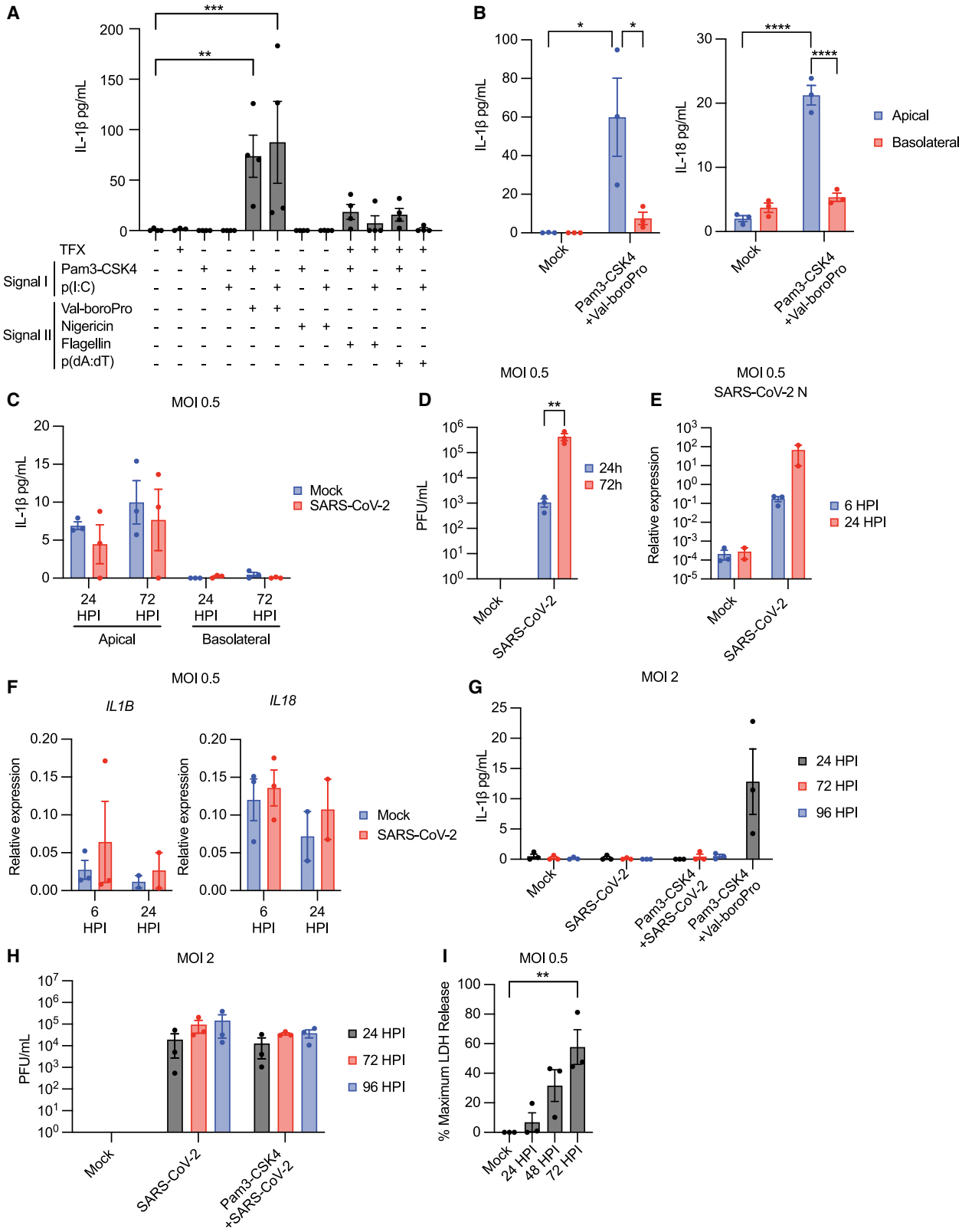

Figure 1. Primary, well-differentiated HAE form inflammasomes and secrete IL-1β but not in response to SARS-CoV-2 infection

(A) IL-1β in pooled HAE supernatants following treatment with indicated stimuli ± transfection (TFX).

(B) IL-1β and IL-18 in HAE supernatants following stimulation.

(legend continued on next page)

Please cite this article in press as: Barnett et al., An epithelial-immune circuit amplifies inflammasome and IL-6 responses to SARS-CoV-2, Cell Host & Microbe (2022), https://doi.org/10.1016/j.chom.2022.12.005

secretion (Figure 1A). HAE were primed by exposure to the triacylated lipopeptide Pam3CysSerLys4 (Pam3-CSK4), a TLR1/2 agonist, or the dsRNA analog polyinosinic-polycytidylic acid (p(I:C)), a TLR3 agonist,[25] and then were exposed to signal II agonists, including nigericin, an NLRP3 inflammasome agonist, the DPP8/9 inhibitor Val-boroPro, an NLRP1 and CARD8 agonist, transfected poly(deoxyadenylic-deoxythymidylic) acid (p(dA:dT)), an AIM2 ligand, or transfected flagellin, a NAIP/NLRC4 agonist.[14,24,50] Val-boroPro but not nigericin stimulated IL-1β release from HAE (Figure 1A), while p(dA:dT) and flagellin stimulated modest responses slightly above baseline. Measurement of cell membrane rupture showed LDH release in conditions stimulating IL-1β secretion, suggesting pyroptotic cell death occurs upon inflammasome activation in HAE (Figure S1A). Apical secretion of both IL-1β and IL-18 was observed after stimulation with Pam3-CSK4 and Val-boroPro (Figure 1B). These results demonstrate HAE can execute pyroptosis and IL-1β secretion and highlight the role of the NLRP1/CARD8 inflammasome in these cultures.

We next assessed whether SARS-CoV-2 infection stimulates IL-1β secretion from HAE. HAE were infected with SARS-CoV-2 at a multiplicity of infection (MOI) of 0.5, and IL-1β secretion was measured after infection. IL-1β release above baseline was not detected in HAE apical washes or basolateral supernatants at 24 or 72 h post-infection (HPI) (Figure 1C). However, viral titers measured in parallel indicated viral replication (Figure 1D), as did measurement of viral RNA transcripts encoding the SARS-CoV-2 nucleocapsid (N) protein (Figure 1E). Additionally, inflammasome cytokines or components expression did not change with infection (Figures 1F, S1B, and S1C). Increasing the MOI or priming HAE cultures prior to infection did not alter this response (Figure 1G). No IL-1β secretion occurred under these conditions, despite viral replication at all time points (Figure 1H). However, SARS-CoV-2 infection did stimulate lytic cell death, as measured LDH release (Figure 1I). Thus, SARS-CoV-2 infection alone or with priming does not promote IL-1β release from ACE2+ HAE.

SARS-CoV-2 infection in the epithelium indirectly activates the inflammasome in leukocytes

SARS-CoV-2 may activate the inflammasome in monocytes and other myeloid cells, despite not stimulating this response in HAE. This may occur directly, through viral replication, or indirectly, through detection of virions and DAMPs generated by viral replication in the epithelium. While leukocytes are not thought to support viral replication, recent reports have suggested various models of inflammasome activation in leukocytes,[38–40] including direct activation of the inflammasome through viral replication.[37,41]

Thus, we first assessed whether SARS-CoV-2 productively replicated in human PBMCs following infection at MOI 0.5. Between 4 and 24 HPI, viral titers present in infected PBMC culture supernatants decreased on average 10-fold (Figure 2A). Similarly, viral RNA transcripts decreased over time (Figure 2B). In contrast, infection in ACE2+ HAE show log-fold increases in viral titer and RNA following infection (Figures 1D and 1E). Decreases in viral titer and RNA over time suggest productive viral replication does not occur in human PBMCs.

While NLRP3 stimulation promoted IL-1β secretion in PBMCs, SARS-CoV-2 infection did not (Figure 2C). *IL1B* mRNA expression, however, was increased at 4 HPI, indicating inflammasome priming (Figure 2D). *IL1B* mRNA expression stimulated by SARS-CoV-2 was more pronounced at MOI 2, and measurement of other inflammasome-related genes showed increases in *AIM2* and *NLRP3* transcripts (Figures 2E and S2A). Thus, SARS-CoV-2 uptake by PBMCs primes multiple inflammasomes.

Next, we systematically tested whether SARS-CoV-2 was a signal I, signal II, or both for inflammasome activation in human PBMCs, measuring IL-1β secretion after SARS-CoV-2 exposure alone or in combination with exogenous signal I or signal II stimuli. Accordingly, PBMCs were pre-treated with a signal I (Pam3-CSK4) and then exposed to SARS-CoV-2, exposed to SARS-CoV-2 alone, or pre-exposed to SARS-CoV-2 and then treated with a signal II (ATP or nigericin). SARS-CoV-2 exposure alone or with a signal I resulted in little IL-1β secretion (Figure 2F). By contrast, infection followed by signal II treatment led to high levels of IL-1β (>2,000 pg/mL on average) secretion. Therefore, SARS-CoV-2 predominantly serves as a signal I for inflammasome activation in primary human PBMCs.

We next investigated which SARS-CoV-2 virion components mediate inflammasome priming. Priming in PBMCs, measured by *IL1B* transcript upregulation, was sensitive to Bay11-7082, an NF-κB inhibitor, and chloroquine, an inhibitor of endosomal/phagosomal acidification, suggesting that these pathways are required for priming (Figure 2G). *IL1B* transcript upregulation was also inhibited by the TLR2 inhibitor C29 (Figure 2G), consistent with reports suggesting TLR2 is required for the pro-inflammatory response to SARS-CoV-2.[26,39,51] Because TLR2 blockade decreased *IL1B* transcript upregulation, we determined whether the SARS-CoV-2 structural proteins S or E stimulated this response, as both are reported to stimulate TLR2.[26,39,51] We observed upregulation of *IL1B* mRNA by E, while S did not (Figure 2H). Consistent with a role in priming, E, but not S, stimulated IL-1β secretion in combination with subsequent ATP treatment (Figure 2I). Thus, E primes inflammasomes via TLR2 stimulation, consistent with another report.[26]

If SARS-CoV-2 is primarily a signal I in PBMCs, then inflammasome activation in PBMCs requires an additional signal II.

(C) IL-1β in HAE supernatants following SARS-CoV-2 infection.
(D) Viral titer from HAE apical wash following SARS-CoV-2 infection.
(E) Viral N RNA expression relative to *ACTB*.
(F) *IL1B* and *IL18* expression relative to *ACTB*.
(G) Apical IL-1β secretion from HAE following SARS-CoV-2 infection or stimulation.
(H) Viral titer from HAE apical wash following infection.
(I) LDH in HAE apical wash following SARS-CoV-2 infection. Data points represent individual HAE donors with bars shown as mean ± SEM. *$p < 0.05$, **$p < 0.01$, ***$p < 0.001$, or ****$p < 0.0001$ calculated by ordinary one-way (A and I) or two-way (B and D) ANOVA followed by Dunnett's (A and I) or Tukey's (B and D) multiple comparison test.
See also Figure S1.

Please cite this article in press as: Barnett et al., An epithelial-immune circuit amplifies inflammasome and IL-6 responses to SARS-CoV-2, Cell Host & Microbe (2022), https://doi.org/10.1016/j.chom.2022.12.005

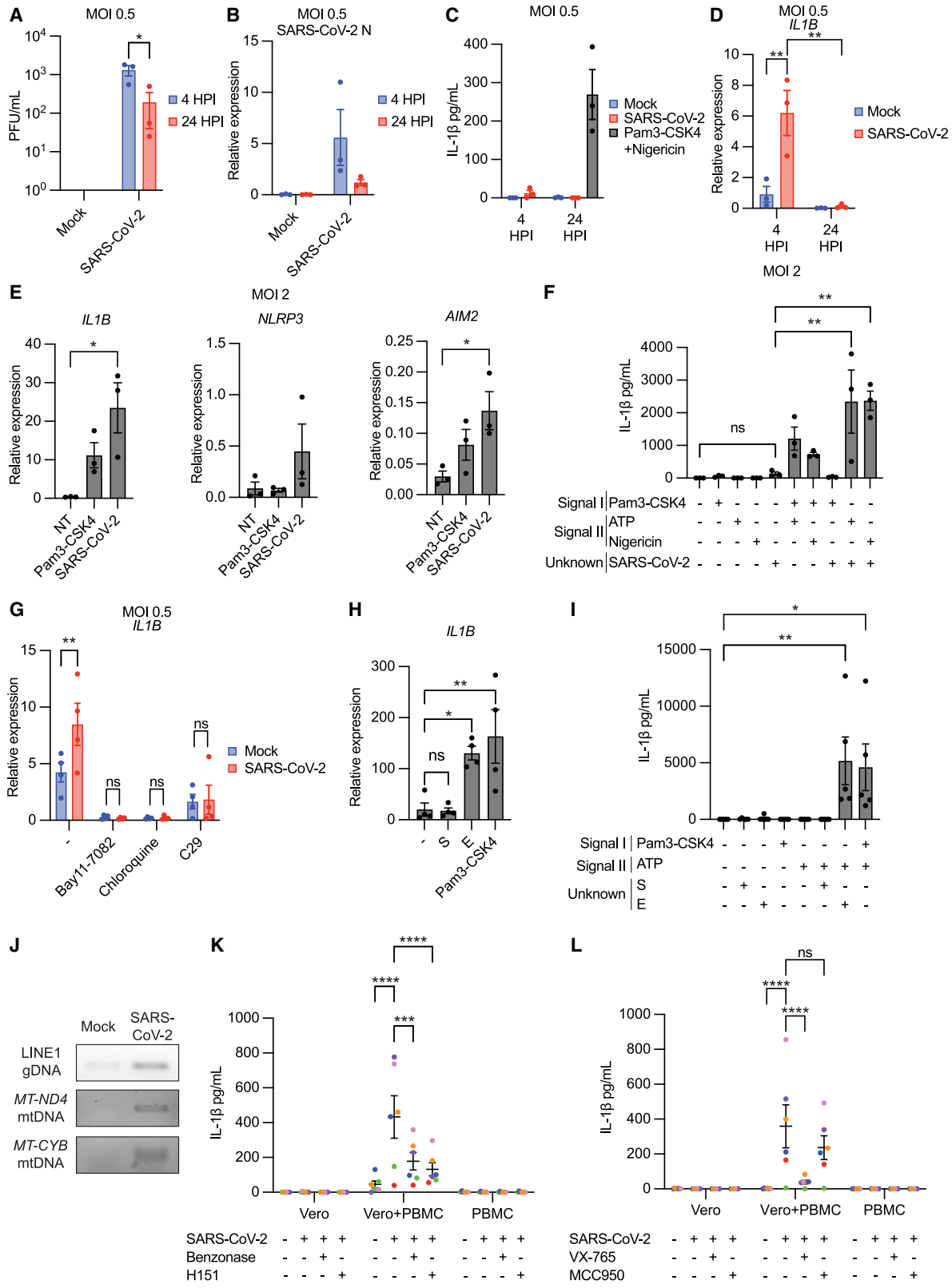

(legend on next page)

Please cite this article in press as: Barnett et al., An epithelial-immune circuit amplifies inflammasome and IL-6 responses to SARS-CoV-2, Cell Host & Microbe (2022), https://doi.org/10.1016/j.chom.2022.12.005

DAMPs released from infected epithelial cells may provide this signal. Genomic DNA encoding long-interspersed nuclear elements (LINE-1) and mitochondrial (mt)DNA encoding mitochondrial genes (*MT-ND4* and *MT-CYB*) were increased in SARS-CoV-2-infected HAE supernatants (Figures 2J and S2B). dsDNA is a well-characterized inflammasome agonist that stimulates the AIM2 and/or NLRP3 inflammasomes, mediated by the cyclic GMP-AMP synthase (cGAS)/stimulator of interferon genes (STING) pathway in humans.[45–47] Its presence in infected HAE supernatants confirms infected cells release inflammasome-stimulatory DAMPs. Therefore, infected epithelial cells produce both signal I (virions) and signal II (dsDNA) to activate the inflammasome in leukocytes.

To model inflammasome activation through cell-cell interaction, we infected or mock-infected the epithelial cell line Vero-E6 with SARS-CoV-2, and 72 HPI, PBMCs were co-cultured with infected or mock-infected cells for 24 h (Figure S2C). Similar to HAE, Vero-E6 cells support SARS-CoV-2 replication (Figure S2D). As a negative control, PBMCs were exposed or mock-exposed to SARS-CoV-2 for 24 h. Only PBMCs co-cultured with infected Vero-E6 cells secreted IL-1β (Figure 2K), indicating infected cells, not virions alone, promote *de novo* inflammasome activation in PBMCs. The extent of this response varied between PBMC donors. Addition of benzonase, a nuclease with activity in a wide range of buffers, abrogated IL-1β release (Figure 2K). This response was also sensitive to H151, an inhibitor of STING, an adaptor protein critical for the interferon and inflammasome responses to intracellular DNA.[45,46] Thus, DNA DAMPs are essential for SARS-CoV-2-mediated inflammasome activation in co-culture.

We then tested the requirement of specific inflammasome components in this system. This response was sensitive to VX-765, a human caspase-1/4 inhibitor, confirming inflammasome-dependent secretion (Figure 2L). However, this response was reduced modestly but not significantly by NLRP3 inhibition, suggesting other or multiple inflammasomes mediate IL-1β release in co-culture. Taken together, these data suggest interactions with SARS-CoV-2-infected epithelial cells, rather than virions alone, stimulate inflammasomes in leukocytes through sensing of DNA DAMPs.

Myeloid cells from COVID-19 autopsy lungs have active inflammasomes but not SARS-CoV-2 antigens

Next, we investigated COVID-19 patient autopsy lungs for inflammasome priming and activation in the alveoli. First, we examined inflammasome priming by RNA *in situ* hybridization (RNA-ISH). Compared with control lungs from donors without pre-existing pulmonary disease, COVID-19 patient lungs exhibited increased expression of *NLRP3*, *AIM2*, and *CASP1* (Figure 3A), driven in part by the influx on myeloid populations into COVID-19 lungs. Consistent with a role in the pulmonary epithelium, *NLRP1* expression in COVID-19 autopsy lungs was comparable to controls (Figure 3A). To assess which cell types expressed these inflammasome components, we utilized fluorescent RNA-ISH to label these transcripts in combination with *CD68*, expressed by macrophages,[52] and *MPO*, expressed by neutrophils.[53] *CASP1*, *NLRP3*, and *AIM2* expressions were primarily associated with $CD68^{+}MPO^{-}$ cells, suggesting that these genes are predominantly expressed in macrophage populations in COVID-19 autopsy lungs (Figure 3B). *NLRP1*, however, was enriched in $CD68^{-}MPO^{-}$ cells (Figure 3B). Multiple epithelial cell types have the *NLRP1* inflammasome,[54,55] and these data indicate its predominance in non-myeloid cell types in the lung. Overall, this increase in inflammasome component gene expression suggests the *NLRP3* and *AIM2* inflammasomes are primed in myeloid populations in COVID-19 autopsy lungs.

Increased inflammasome gene expression indicates inflammasome priming by signal I, but not activation by signal II. Therefore, we investigated ASC speck formation in these lungs by immunohistochemistry because this adaptor protein forms a large, perinuclear speck upon inflammasome activation and oligomerization.[56] Compared with controls, COVID-19 autopsy lungs had an increased frequency of ASC specks, showing inflammasome activation *in vivo* (Figure 3C). These specks were present in several myeloid populations, including CD68+ and MPO+ cells, but most predominantly in CD11c+ cells, a marker of many myeloid subpopulations including dendritic cells (DCs) and alveolar macrophages[57] (Figure 3D). To assess contributions of the alveolar epithelium, we investigated ASC speck formation in ABCA3+ alveolar type II cells, which support SARS-CoV-2 replication in the alveoli,[42] and found ASC specks were largely absent from ABCA3+ cells (Figure S3A).

Figure 2. SARS-CoV-2 primes the inflammasome in PBMCs, while co-culture of PBMCs with infected epithelial cells fully activates inflammasome-mediated IL-1β secretion

(A) Viral titer from PBMC supernatants.
(B) Viral N RNA expression in PBMC relative to *ACTB*.
(C) IL-1β release from PBMC supernatants following SARS-CoV-2 infection or stimulation.
(D) *IL1B* transcript expression relative to *ACTB*.
(E) Indicated transcript expression relative to *ACTB* after 4-h SARS-CoV-2 exposure.
(F) IL-1β in PBMC supernatants following SARS-CoV-2 exposure alone or in combination with indicated signal I or II stimuli.
(G) *IL1B* transcript expression relative to *ACTB* in PBMC at 4 HPI with SARS-CoV-2 ± Bay11-7082 (10 μM), chloroquine (10 μM), and C29 (25 μM).
(H) *IL1B* expression relative to *ACTB* following 3-h treatment with 1 μg/mL S, E, or Pam3-CSK4.
(I) IL-1β secretion from PBMCs following 3-h treatment described in (H) and subsequent ATP treatment (5 mM; 1 h).
(J) PCR-amplified detection of dsDNA in HAE supernatants ± SARS-CoV-2 (MOI 0.5) at 24 HPI.
(K and L) IL-1β in supernatants after infection in PBMCs, Vero-E6 cells, or co-culture of PBMCs with infected Vero-E6 cells (K) ± benzonase (20 units/mL) or H151 (10 μM) and (L) ± VX-765 (20 μg/mL) or MCC950 (5 μM). Data point color indicates specific PBMC donors and matched Vero-E6 values across conditions. Data points on graphs represent individual PBMC donors with bars or lines shown as mean ± SEM. *$p < 0.05$, **$p < 0.01$, ***$p < 0.001$, or ****$p < 0.0001$ as calculated by ordinary one-way (E, F, H, and I) or two-way (A, D, G, K, and L) ANOVA followed by Tukey's (A, D, F, K, and L), Dunnet's (E, H, and I), or Sidak's (G) multiple comparison test.
See also Figure S2.

Please cite this article in press as: Barnett et al., An epithelial-immune circuit amplifies inflammasome and IL-6 responses to SARS-CoV-2, Cell Host & Microbe (2022), https://doi.org/10.1016/j.chom.2022.12.005

CellPress

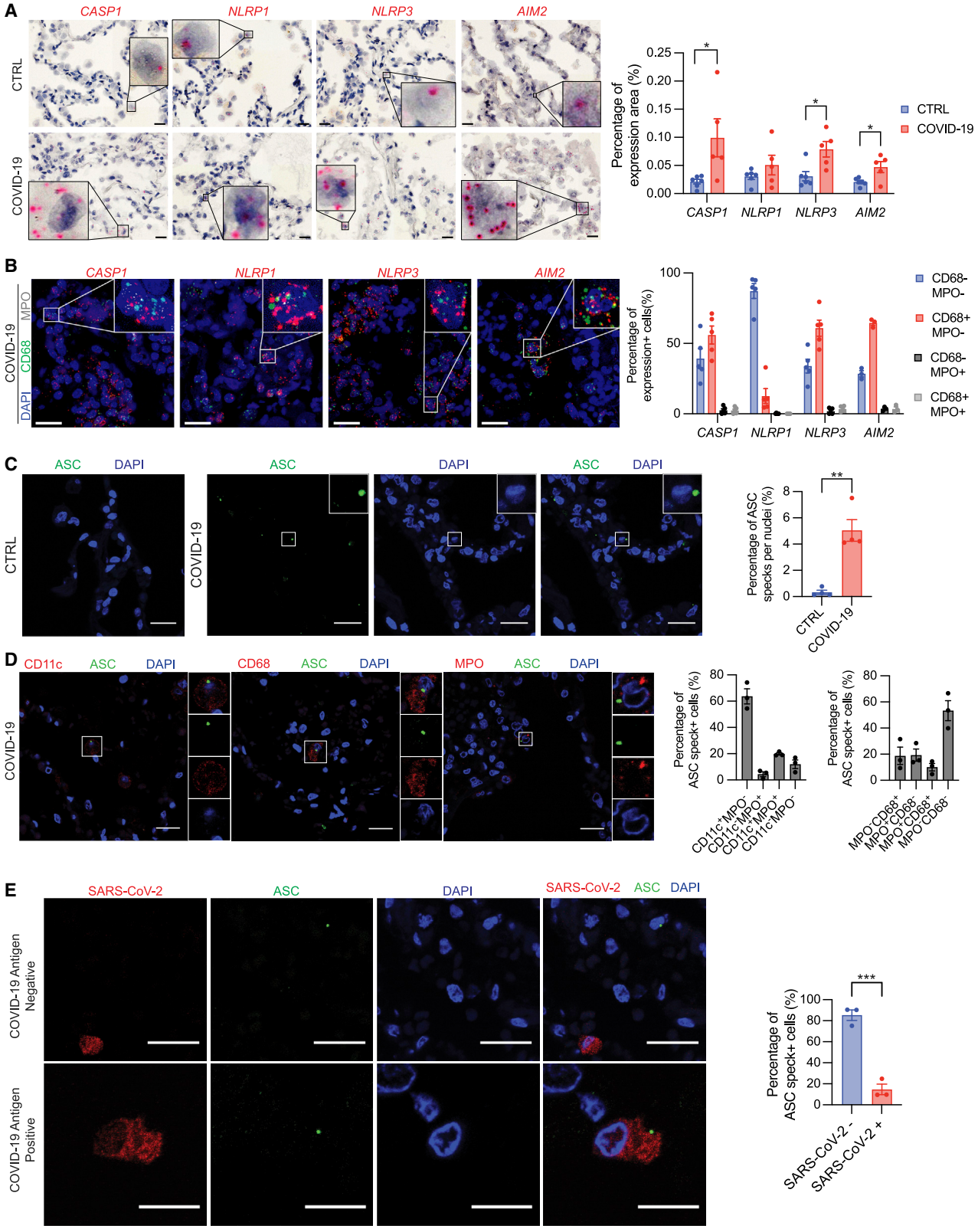

Figure 3. Myeloid cells in COVID-19 autopsy lungs show hallmarks of inflammasome priming and activation primarily in cells lacking SARS-CoV-2 antigen

(A) Representative images (left) and quantification (right) of RNA-ISH in control and COVID-19 autopsy lungs.

(legend continued on next page)

Please cite this article in press as: Barnett et al., An epithelial-immune circuit amplifies inflammasome and IL-6 responses to SARS-CoV-2, Cell Host & Microbe (2022), https://doi.org/10.1016/j.chom.2022.12.005

Previous reports note SARS-CoV-2 antigens in myeloid cells.[38,40,41] However, the relative proportions of ASC speck+ myeloid cells containing viral antigens at the site of infection in humans remains unclear. Therefore, we determined whether cells with ASC specks also contained SARS-CoV-2 antigens in COVID-19 autopsy lungs. On average, over 80% ASC speck+ cells lacked SARS-CoV-2 antigens (Figure 3E). Furthermore, CD68+ and MPO+ cells infrequently colocalized with SARS-CoV-2 antigen (Figure S3B), though some myeloid cells do contain SARS-CoV-2, corroborating previous observations.[38,40,41] Because many myeloid cells are professional phagocytes, uptake of infected cells and virions containing SARS-CoV-2 antigens during infection is expected and not confirmatory of viral infection or replication. These data suggest uninfected myeloid bystanders mediate a majority of the inflammasome response in fatal COVID-19.

scRNA-seq analysis of patient BALF samples reveals a heightened but discordant inflammasome response in severe COVID-19

Active inflammasomes in COVID-19 autopsy lungs demonstrates responses in fatal disease but does not allow for comparison with mild disease. Therefore, we conducted a meta-analysis of COVID-19 patient scRNA-seq data to determine whether COVID-19 disease states showed differential inflammasome priming.[9,58] After filtering, we analyzed 117,497 high-quality transcriptomes from the BALF of three healthy donors, five mild/moderate COVID-19 patients, and 26 severe COVID-19 patients. We utilized shared nearest neighbor, a graph-based clustering method, to identify unique cell populations and visualized the results via uniform manifold approximation and projection (UMAP) analysis (Figure 4A). To boost statistical power and incorporate new studies, we projected cells from additional COVID-19 and healthy patient scRNA-seq datasets onto this reference space (Figure S4A).[59–61] In total, we analyzed over 300,000 high-quality transcriptomes from the BALF of 13 healthy donors, five mild/moderate COVID-19 patients, and 50 severe COVID-19 patients.

We identified 22 unique cell clusters with varied distribution by disease state (Figures 4B and S4B), including 11 unique myeloid populations (Figure 4A). Epithelial cells were predominantly observed in COVID-19 patients, not healthy individuals, and present mostly in severe patients (Figure 4B), likely due to dissociation of infected cells from the lung epithelium. Distribution of myeloid cells within specific clusters shifted between disease states, suggesting myeloid characteristics change with COVID-19 disease status. HLA-DR^{low} myeloid cells were enriched (cluster 2; Figures 4A and 4B) in severe patients, a population previously observed in severe COVID-19.[4,10,62]

To gain a general understanding of the inflammasome pathway, we assigned each cell an "inflammasome score" based inflammasome-related gene expression (*IL1B*, *IL18*, *NLRP1*, *NLRP3*, *NLRC4*, *NLRP6, AIM2*, *NAIP*, *MEFV*, *CASP1*, *CASP4*, *CASP5*, *PYCARD*, and *GSDMD*), a technique used to define cell pathway programs in other scRNA-seq datasets[63] (Figure 4C). To control for cell-specific effects, these scores were normalized by subtracting a control score defined by a gene set with comparable expression distribution, creating $\log_{10}$ inflammasome scores ranging between −0.84 and 1.51.[64] Across all clusters, the mean inflammasome score was −0.05. The myeloid cluster 14 had the highest mean inflammasome score of 0.03926 with increased expression levels of *IL1B*, *CASP1*, and *CASP4* compared with other clusters (Figures 4C and S4C). Other myeloid clusters with heightened *IL1B* expression, including the HLA-DR^{low} cluster 2, also had high inflammasome scores. In contrast, clusters 18, ciliated epithelial cells, 12, secretory epithelial cells, and 9, T cells, had the lowest inflammasome scores of −0.262, −0.163, and −0.193, respectively. Myeloid cells from both mild/moderate and severe COVID-19 patients tended to have increased inflammasome scores compared with healthy donors, indicating inflammasome priming occurs universally in COVID-19 (Figure 4D). Thus, myeloid populations, including those expanded in severe disease, dictate the inflammasome response in COVID-19.

The range of inflammasome scores within individual clusters in severe disease varied widely (Figure 4E). This was most apparent in the HLA-DR^{low} cluster 2 where inflammasome scores in severe patients encompassed the range of the entire dataset. We found inflammasome score variance increased stepwise by disease state with a mean of 0.01007 in healthy donors, 0.02955 in mild/moderate COVID-19, and 0.04140 in severe COVID-19 (Figure 4F). In myeloid clusters 14 and 15, variance significantly increased between mild/moderate and severe COVID-19, and inflammasome score variance was significantly increased in every myeloid cluster between healthy donors and severe COVID-19 patients (Figure S4D). Thus, severe COVID-19 showed higher variance of inflammasome scores compared with other disease states. Many cells from severe patients showed dramatically higher or lower scores than observed in mild/moderate disease. This disparate inflammasome response may indicate a loss of regulation of the inflammasome in severe COVID-19.

Given such profound heterogeneity, comparisons of mean inflammasome scores between disease states using linear mixed models approach showed no apparent differences. However, the wide range of inflammasome scores in severe disease indicates subpopulations of myeloid cells may have increased inflammasome gene expression. To compare the 75th percentile of inflammasome scores in each group, we employed a linear quantile mixed model to determine if the 75th quantile of inflammasome score changed between disease

(B) Representative images (left) and quantification (right) of fluorescent dual RNA-ISH labeling indicated inflammasome genes with *CD68* or *MPO*.
(C) Representative maximum Z projection (left) and quantification (right) of ASC immunostaining in control or COVID-19 autopsy lungs.
(D) Representative images of ASC specks with cell-type markers in COVID-19 autopsy lungs (left) and quantifications (right).
(E) Representative images of COVID-19 autopsy lungs of ASC specks in combination with SARS-CoV-2 antigen and quantification (right). All scale bars represent 20 μm. Data points on graphs represent individual donor lungs with bars shown as mean ± SEM. *$p < 0.05$, **$p < 0.01$, ***$p < 0.001$, or ****$p < 0.0001$ calculated by Student's two-tailed, unpaired t test.
See also Figure S3.

Please cite this article in press as: Barnett et al., An epithelial-immune circuit amplifies inflammasome and IL-6 responses to SARS-CoV-2, Cell Host & Microbe (2022), https://doi.org/10.1016/j.chom.2022.12.005

CellPress

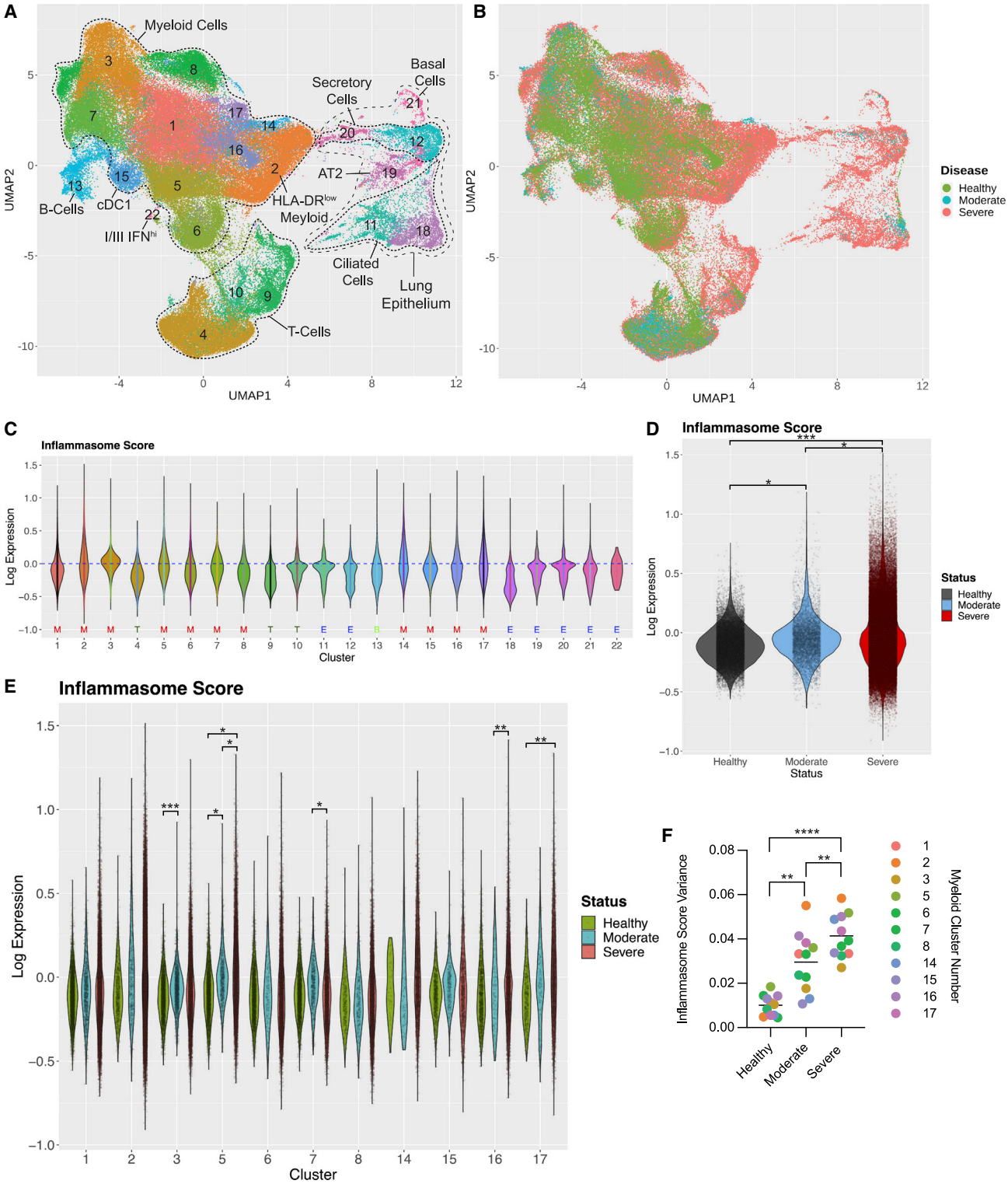

Figure 4. Meta-analysis of COVID-19 patient BALF scRNA-seq reveals differential expression of inflammasome pathway by disease state

(A) UMAP of healthy and COVID-19 patient BALF scRNA-seq from pooled studies (healthy: n = 3; mild/moderate COVID-19: n = 5; severe COVID-19: n = 26). Each dot represents a cell, and each dot is colored according to cluster identity. Clusters are annotated by cell type. ‡ denotes the HLA-DR^{low} myeloid population.

(B) UMAP shown in (A) but colored by patient disease state (healthy, mild/moderate, or severe).

(legend continued on next page)

Please cite this article in press as: Barnett et al., An epithelial-immune circuit amplifies inflammasome and IL-6 responses to SARS-CoV-2, Cell Host & Microbe (2022), https://doi.org/10.1016/j.chom.2022.12.005

states and found significant disease effects in the 75th quantile of inflammasome scores (Figure 4D). Overall, the differences observed in inflammasome score variance between disease states highlight the heterogeneity inflammasome gene expression in severe COVID-19, while increased expression of these genes in the 75th quantile of severe patient myeloid cells indicates a subset of cells in severe disease have exacerbated inflammasome gene expression not observed in other disease states. This priming was only partially dependent on SARS-CoV-2 transcripts, since only a modest correlation between viral genomes and inflammasome score was observed (Figure S4E).

We next examined expression of individual genes. As described above, severe COVID-19 has high variance in inflammasome gene expression levels. Variation within samples (intra-patient variance) and variation between samples (inter-patient variance) contribute to this phenomenon. A major factor contributing to variation within samples is large numbers of gene dropout (zero RNA read count for some genes in some cells), an occurrence universally present in scRNA-seq datasets. However, a myriad of clinical and environmental factors, including age, gender, pre-existing conditions, batch preparation conditions, and course of treatment, contribute to inter-patient variance. These differences cannot be properly controlled with the small number of patients surveyed at single-cell levels. Therefore, we utilized a linear quantile mixed model treating sample identity as a random effect to identify inflammasome pathway genes differentially regulated by COVID-19 disease state. Because severe COVID-19 pathology involves increased inflammation, we compared inflammasome gene expression levels at the 75th quantile, assessing differences between the highest-expressing cells.

IL1B expression was exacerbated in myeloid cells from severe COVID-19 patients at orders of magnitude higher than mild/moderate COVID-19 (Figure 5A). While no differences were observed between healthy and mild/moderate COVID-19, the 75th quantile of *IL1B* expression was increased in severe disease versus healthy controls in several clusters and versus mild/moderate disease in clusters 2 and 14 (Figure 5A). Other genes shared among inflammasome pathways, *IL18*, *CASP1*, and *GSDMD*, had less variable expression though cells with extremely high levels of expression were observed in severe COVID-19 (Figures S5A–S5C). Thus, a subset of myeloid cells in severe COVID-19 express high levels of shared inflammasome genes.

Specific inflammasome sensors followed a similar pattern across disease states. *NLRP3* showed heightened expression in severe COVID-19 in several myeloid clusters compared with other disease states (Figure 5B). Similarly, the 75th quantile of *AIM2* expression was increased in specific myeloid clusters in severe and mild/moderate COVID-19 compared with healthy donors (Figure 5C). *MEFV*, the gene encoding Pyrin, expression was aggravated in several myeloid clusters in severe COVID-19, showing dynamic changes in both COVID-19 disease states (Figure 5D). Likewise, only myeloid cells in severe COVID-19 showed high levels of *NLRP6* expression (Figure S5D). Additionally, the non-canonical caspase *CASP4* showed exacerbated expression in some myeloid clusters in severe COVID-19 (Figure S5E).

Our scRNA-seq meta-analysis revealed differential inflammasome pathway expression between COVID-19 disease states. Myeloid cells from patients with mild/moderate COVID-19 showed lower variance in inflammasome gene expression and uniform enrichment of these genes over a healthy baseline. Since the inflammasome is protective in other respiratory viral infections, this uniform response may promote disease resolution in mild/moderate disease. However, in severe disease, myeloid cells showed striking heterogeneity with a subset of cells exhibiting exacerbated expression to levels not observed in mild/moderate disease. Such cells from severe patients may be able to mount a powerful inflammasome cytokine response in severe COVID-19.

SARS-CoV-2 infection in HAE stimulates IL-1β release from PBMC causing IL-6 release from both cell types

Both L-1β and IL-6 are thought to contribute to COVID-19 fatalities. IL-6 secretion can be induced by multiple mechanisms,[65] and COVID-19 patients receiving IL-1 receptor blockade therapy have lower levels of circulating IL-6.[11] Therefore, we investigated whether inflammasome-mediated IL-1β secretion amplified IL-6 production, too.

We assessed whether SARS-CoV-2 infection induced *IL6* expression in HAE and/or PBMCs. At 4 HPI, we saw no increase in *IL6* expression in PBMCs (Figure S6A), unlike *IL1B* measured in parallel (Figure 2D). In HAE, *IL6* transcripts did not increase in at 6, 48, or 72 HPI, similar to acute stimulation with Pam3-CSK4 (Figures S6B and S6C). Thus, neither viral replication in epithelial cells nor PBMC uptake of virions stimulates increases in *IL6* transcripts at acute time points, suggesting other mechanisms promote *IL6* upregulation.

We then investigated whether IL-1β stimulation induced *IL6* expression. PBMCs or HAE were treated with 100 pg/mL or 1 ng/mL IL-1β and assessed *IL6* expression at 4 and 24 h post-treatment (HPT). IL-1β increased *IL6* expression in PBMCs (Figure 6A), demonstrating that IL-1β, but not SARS-CoV-2 virions, induces *IL6* expression in this cell type. However, increases in *IL6* expression following IL-1β treatment in HAE were modest (Figure 6B).

In parallel, we measured IL-6 secretion. Both PBMCs and HAE secreted IL-6 following IL-1β stimulation, but the extent differed between cell types (Figure 6C). PBMCs treated with IL-1β showed some IL-6 secretion at 24HPT with an average around

(C) Inflammasome scores for each cluster of the UMAP shown in (A). General cluster identity indicated below cluster number: M, myeloid cells; T, T cells; B, B cells, and E, epithelial cells.
(D) Inflammasome scores for all myeloid cells in COVID-19 disease states and healthy patients. Each dot represents a cell.
(E) Inflammasome scores for individual cells (individual points) within each myeloid cluster across COVID-19 disease states.
(F) Inflammasome score variance within each myeloid cluster by disease state. (C)–(F) include projected datasets. Statistical calculations are described in the STAR Methods and text, except for (F) which was determined by paired two-sided t test *p < 0.05, **p < 0.01, ***p < 0.001, or ****p < 0.0001.
See also Figure S4.

Please cite this article in press as: Barnett et al., An epithelial-immune circuit amplifies inflammasome and IL-6 responses to SARS-CoV-2, Cell Host & Microbe (2022), https://doi.org/10.1016/j.chom.2022.12.005

CellPress

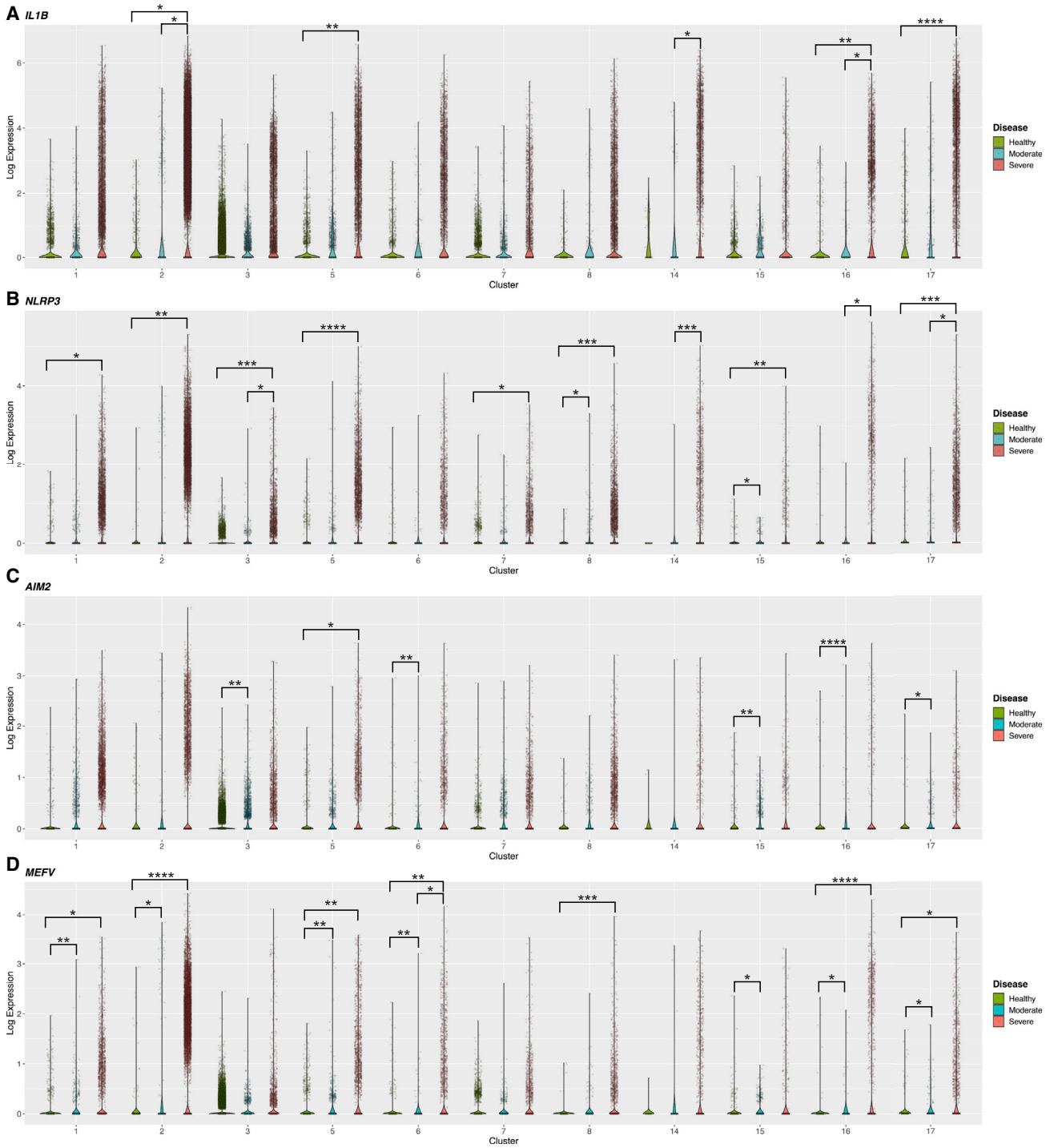

Figure 5. Enriched expression of inflammasome genes and cytokines in specific myeloid subpopulations in severe COVID-19

Violin plots of normalized gene expression in each myeloid cluster by disease status. Includes projected data. Each cell shown by an individual dot. Each panel shows a different gene: (A) *IL1B*, (B) *NLRP3*, (C) *AIM2*, and (D) *MEFV*. *p < 0.05, **p < 0.01, ***p < 0.001, or ****p < 0.0001. Statistical calculations described in STAR Methods and text.

See also Figure S5.

1,000 pg/mL. However, pooled supernatants from HAE demonstrated a strong IL-6 response at 24 HPT with an average of over 7, 000 pg/mL (Figure 6C).

These data suggest a model in which SARS-CoV-2 infection in the epithelium triggers inflammasome activation in myeloid bystanders, and in turn the IL-1β released stimulates IL-6

Please cite this article in press as: Barnett et al., An epithelial-immune circuit amplifies inflammasome and IL-6 responses to SARS-CoV-2, Cell Host & Microbe (2022), https://doi.org/10.1016/j.chom.2022.12.005

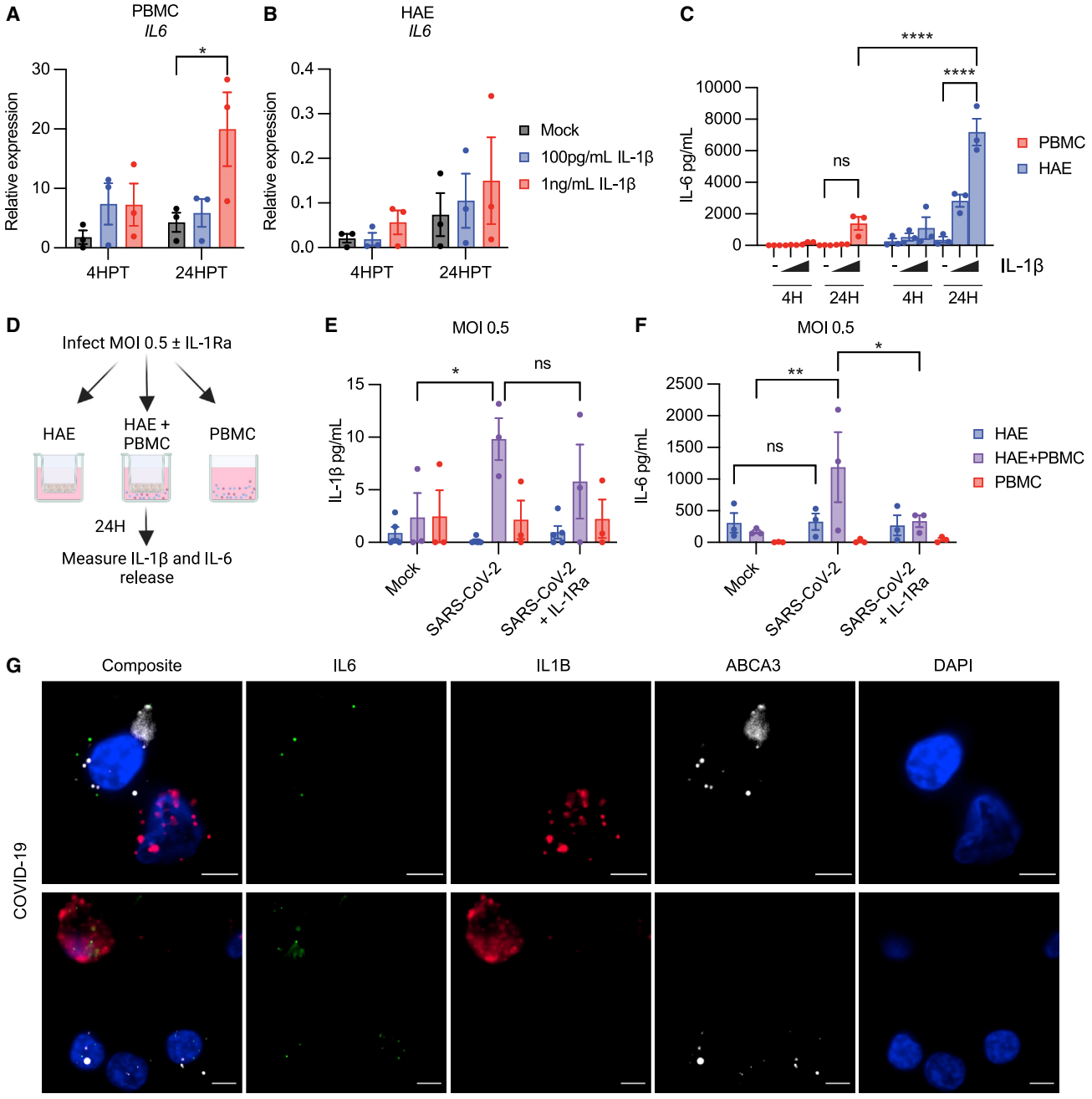

Figure 6. IL-1β stimulates IL-6 secretion from PBMCs and HAE

(A–C) PBMCs or HAE treated with 100 pg/mL or 1 ng/mL IL-1β. (A) *IL6* transcripts relative to *ACTB* in PBMCs (B) *IL6* expression relative to *ACTB* in HAE. (C) IL-6 secretion from pooled HAE supernatants or PBMCs.

(D) Schematic of HAE-PBMC co-culture experiment. Created with BioRender.com.

(E) IL-1β in supernatants from experiment in (D).

(F) IL-6 in supernatants from experiment in (D).

(G) Representative images of RNA-ISH in COVID-19 autopsy lungs. Scale bar represents 5 μm. Data points on graphs represent individual donors (HAE or PBMC) or donor pairs (HAE + PBMC) with bars shown as mean ± SEM. *$p < 0.05$, **$p < 0.01$, ***$p < 0.001$, or ****$p < 0.0001$ as calculated by two-way ANOVA followed by Dunnett's (A and B) or Tukey's multiple comparison test (C, E, and F).

See also Figure S6.

secretion from both cell types. To test this, we developed a primary, human co-culture system of HAE and PBMC and measured IL-1β and IL-6 production during SARS-CoV-2 infection with or without the IL-1 receptor antagonist (IL-1Ra) (Figure 6D). Consistent with our previous observations (Figure 2K), IL-1β secretion only increased upon co-culture of HAE and

Please cite this article in press as: Barnett et al., An epithelial-immune circuit amplifies inflammasome and IL-6 responses to SARS-CoV-2, Cell Host & Microbe (2022), https://doi.org/10.1016/j.chom.2022.12.005

PBMC during SARS-CoV-2 infection (Figure 6E). Similar to IL-1β, IL-6 secretion only increased during SARS-CoV-2 infection in co-culture (Figure 6F). SARS-CoV-2-stimulated IL-6 production in the co-culture setting depended on IL-1, as IL-1Ra fully blocked IL-6 secretion. This intercellular communication circuit was observed in COVID-19 autopsy lungs, where an *IL6*+ *ABCA3*+ alveolar type II epithelial cell was adjacent to a non-epithelial *IL1B*+ or *IL1B*+*IL6*+ cell (Figure 6G, lower panels). Therefore, a bi-directional communication loop between the infected epithelium and immune bystanders promotes production of IL-1β and IL-6 during SARS-CoV-2 infection.

DISCUSSION

Pro-inflammatory cytokines are critical to mount an adaptive immune response and contain infection, yet blockade of IL-1 or IL-6 signaling in patients with severe disease promotes positive outcomes in COVID-19.[11–13,66] Such contrasting functions underscores the necessity to understand how these cytokines are produced during infection. Here, we report inflammation driven by inflammasome-mediated IL-1β secretion is a product not only of viral infection but also crosstalk between the infected epithelium and myeloid bystanders. Integrated detection of virions and epithelial DAMPs produced during infection activates the inflammasome in myeloid cells. IL-1β release then potentiates IL-6 secretion from both cell types with a potent IL-6 response from the epithelium. Such a circuit of bi-directional cytokine amplification can potentially result in the uncontrolled cytokine storm that accompanies COVID-19 fatalities.

Several groups reported that SARS-CoV-2 replication directly activates the inflammasome in leukocytes,[37–41] but this requires additional exogenous stimuli like bacterial ligands or non-neutralizing antibodies and still only occurs in a small proportion of cells.[38–40] Due to lack of ACE2 expression,[34–36] SARS-CoV-2 replication events in leukocytes are infrequent and abortive.[40,67] Indeed, in the absence of exogenous factors, we did not observe productive viral replication or IL-1β secretion upon SARS-CoV-2 infection in PBMCs. Similarly, HAE, which support productive viral replication and have functional inflammasomes, do not release IL-1β following infection, possibly due to viral antagonism of the pathway.[43] Therefore, while SARS-CoV-2 replication can stimulate modest responses under certain conditions, it is insufficient to drive robust IL-1β release. Furthermore, disease kinetics indicate viral replication is not the lone driver of severe COVID-19 pathology, as viral titers wane in late disease while inflammation continues to mount.[68] Thus, it is paramount to understand how SARS-CoV-2 infection promotes IL-1β release beyond the direct sensing of viral replicative activity within an infected cell.

Here, we show how cell-cell interactions and DAMPs amplify inflammasome responses during SARS-CoV-2 infection. SARS-CoV-2 virions prime the inflammasome pathway in myeloid cells through TLR2-dependent sensing of the SARS-CoV-2 E protein.[26] Then, infected epithelial cells release DAMPs that supply a signal II to initiate IL-1β release. A key DAMP in this process is the well-characterized inflammasome agonist dsDNA. SARS-CoV-2-infected HAE release both genomic and mitochondrial dsDNA, and co-culture of leukocytes with infected epithelial cells promotes IL-1β release, while infection in either cell type in isolation does not. Addition of nuclease or inhibition of STING, an adaptor protein essential for the interferon and inflammasome responses to DNA in humans,[45,46] abrogated IL-1β release in co-culture. Thus, DNA DAMPs are critical for IL-1β release in this system. Furthermore, while blockade of caspase-1 activity was blocked IL-1β release in this system, NLRP3 inhibition had a modest and insignificant effect. This suggests the AIM2 inflammasome, previously observed in COVID-19 patient samples,[40] may also contribute to response. Thus, viral replication in the epithelium provides both signals I and II to stimulate the inflammasome in myeloid bystanders through production of virions and release of DNA DAMPs. Such a model explains how inflammasome activation occurs during early infection in naive individuals and how this response is exacerbated in late disease, as sustained infection leads to significant damage to the lung epithelium.[69]

Observations in COVID-19 patients corroborated these *in vitro* findings. Active inflammasomes, evidenced by ASC speck formation, were prominent in multiple myeloid cell types in COVID-19 autopsy lungs. However, these ASC specks were rarely found in epithelial cells and infrequently colocalized with viral antigens. Thus, the bulk of inflammasome activation in fatal COVID-19 occurs in myeloid bystanders, not cells with active viral replication.

Meta-analysis of patient BALF scRNA-seq data permitted high-resolution dissection of inflammasome priming in COVID-19. We found that inflammasome priming occurs universally in COVID-19, but the extent of priming varied between disease states and was exceptionally discordant in severe COVID-19. Mild/moderate COVID-19 patients show modest increases in inflammasome cytokine and component gene expression in myeloid cells. In contrast, priming in severe disease showed striking heterogeneity with high variance in inflammasome-related gene expression, indicative of a loss of regulation. Maximal expression of inflammasome-related genes was significantly increased in severe COVID-19 patients' myeloid cells, suggesting some cells in severe COVID-19 are hyper-primed for inflammasome activation. Thus, while the inflammasome response is not unique to severe disease, a discordant, hyperactive response may contribute to its pathology. Clinical practices reflect this notion, as effective IL-1 receptor blockade therapy relies on patient indicators of disease severity.[11]

Epithelial-immune interactions do not only amplify IL-1β release in COVID-19. In COVID-19 patients, IL-1 receptor blockade therapy also decreases circulating IL-6,[11] and *in vitro*, we find that co-culture of infected HAE and PBMCs stimulates IL-6 release in an IL-1-dependent manner. Though both PBMCs and HAE secrete IL-6, HAE secreted much higher amounts, despite less dynamic changes in *IL6* mRNA expression. This cautions against relying solely on transcriptional data and indicates a need to understand cytokine release in non-immune cell types.

As a whole, our work underscores the importance of immune-stromal interaction during SARS-CoV-2 infection. Viral infection alone is insufficient to generate robust pro-inflammatory responses in either cell type in isolation, but innate immune sensing of infection in the epithelium by leukocytes promotes production of IL-1β and IL-6. This indirect model of cytokine production offers insight into the heterogeneity observed in

patient responses, as patient-derived factors, namely DAMPs, contribute to both the IL-1β and IL-6 responses in COVID-19. Such a model may extend to other viral infections with differential pro-inflammatory responses in patients. Indeed, epithelial-immune crosstalk may govern many aspects of the local immune response to viruses, mandating further study of these interactions during infection and how they are altered in high-risk patient groups.

STAR★METHODS

Detailed methods are provided in the online version of this paper and include the following:

- KEY RESOURCES TABLE
- RESOURCE AVAILABILITY
  - Lead contact
  - Materials availability
  - Data and code availability
- EXPERIMENTAL MODEL AND SUBJECT DETAILS
  - Human subjects
  - Primary cell isolation and culture
  - Vero cell line culture
- METHOD DETAILS
  - Inflammasome stimulation
  - IL-1β or Protein/Ligand stimulation
  - Viral infections
  - RT-qPCR
  - PCR detection of DNA in supernatants
  - Plaque assay
  - Integrated scRNA-seq meta-analysis
  - Immunohistochemistry
  - RNA *in situ* hybridization (RNA-ISH)
- QUANTIFICATION AND STATISTICAL ANALYSIS
  - Image quantification
  - Statistical analysis
  - scRNAseq Statistical analysis

SUPPLEMENTAL INFORMATION

Supplemental information can be found online at https://doi.org/10.1016/j.chom.2022.12.005.

ACKNOWLEDGMENTS

This work is supported by NIH grants R56 AI158314, R01 AI158314, AI029564, AI141333, and CA232109 to J.P.-Y.T.; NCI T32CA071341 to K.C.B.; R.C.B. and T.A. are supported by UH3 HL123645, R01 HL136961, P30 DK 065988, P01 HL108808, and BOUCHE19R0; K.O. and R.C.B. are supported by BOUCHE19XX0; K.O. is supported by OKUDA20G0 from the Cystic Fibrosis Foundation; M.T.H., S.A.T.-B., and J.F.L. are supported by NC Policy Collaboratory, R01AI157253, and U19 AI100625; NSF GRFP 2019255197 to J.F.L. T.A. is a Japan Society for the Promotion of Science Overseas Research Fellow. Y.X. is supported by NSF DMS-191290 and NSF IOS 2107215. Y.X. and Y.L.L. are supported by NIH grants R01DE026728 and R01DE031951. HAE culture reagents were provided by the Marsico Lung Institute Tissue Procurement and Cell Culture Core supported by NIH grant DK065988 and Cystic Fibrosis Foundation grant BOUCHR19R0. Some BSL3 work was performed in the Duke Regional Biocontainment Laboratory (Duke RBL), which received partial support for construction from NIH/NIAID (UC6AI058607). Graphical abstract and Figure 6D created using Biorender.com. We would like to thank Ting lab members for helpful discussion.

AUTHOR CONTRIBUTIONS

K.C.B., Y.X., and T.A. contributed equally to this manuscript. Y.L.L., R.C.B., and J.P.-Y.T. also contributed equally to this manuscript. J.P.-Y.T. and K.C.B. conceived of the study. K.C.B. and J.P.-Y.T. wrote the manuscript. R.C.B., T.A., Y.L.L., and Y.X. edited the manuscript. K.C.B., T.A., Y.X., R.C.B., Y.L.L., and J.P.-Y.T. designed experiments. T.H.O., G.D.S., S.H.R., M.T.H., and S.A.T.-B. contributed input to experimental design. K.C.B., S.A.T.-B., J.F.L., D.S., and T.H.O. performed the BSL3 experiments. T.A., K.O., and R.C.G. contributed lung samples, performed RNA-ISH, and immunofluorescent staining. K.C.B. and T.A. captured images of stained lung samples. K.C.B., H.G., K.L., and S.Y. executed the other experiments and analyzed data. K.C.B., S.H.R., and K.L. established and maintained HAE cultures. Y.X., Y.L.L., and K.C.B. performed the scRNA-seq meta-analysis.

DECLARATION OF INTERESTS

J.P.-Y.T. is a cofounder of IMMvention Therapeutix, which works on inflammasome inhibitors.

Received: June 29, 2022
Revised: October 12, 2022
Accepted: December 3, 2022
Published: December 9, 2022

REFERENCES

1. Zhou, F., Yu, T., Du, R., Fan, G., Liu, Y., Liu, Z., Xiang, J., Wang, Y., Song, B., Gu, X., et al. (2020). Clinical course and risk factors for mortality of adult inpatients with COVID-19 in Wuhan, China: a retrospective cohort study. Lancet *395*, 1054–1062. https://doi.org/10.1016/S0140-6736(20)30566-3.
2. Blanco-Melo, D., Nilsson-Payant, B.E., Liu, W.-C., Uhl, S., Hoagland, D., Møller, R., Jordan, T.X., Oishi, K., Panis, M., Sachs, D., et al. (2020). Imbalanced host response to SARS-CoV-2 drives development of COVID-19. Cell *181*. 1036–1045.e9. https://doi.org/10.1016/j.cell.2020.04.026.
3. Lucas, C., Wong, P., Klein, J., Castro, T.B.R., Silva, J., Sundaram, M., Ellingson, M.K., Mao, T., Oh, J.E., Israelow, B., et al. (2020). Longitudinal analyses reveal immunological misfiring in severe COVID-19. Nature *584*, 463–469. https://doi.org/10.1038/s41586-020-2588-y.
4. Wilk, A.J., Rustagi, A., Zhao, N.Q., Roque, J., Martínez-Colón, G.J., McKechnie, J.L., Ivison, G.T., Ranganath, T., Vergara, R., Hollis, T., et al. (2020). A single-cell atlas of the peripheral immune response in patients with severe COVID-19. Nat. Med. *26*, 1070–1076. https://doi.org/10.1038/s41591-020-0944-y.
5. Channappanavar, R., and Perlman, S. (2017). Pathogenic human coronavirus infections: causes and consequences of cytokine storm and immunopathology. Semin. Immunopathol. *39*, 529–539. https://doi.org/10.1007/s00281-017-0629-x.
6. Yifan, Q., Chao, H., Kun, W., Peng, H., Runsheng, W., Jiang, L., Tianzhi, L., Rongyu, P., Qinyong, H., Yu, S., et al. (2021). Cytokine release syndrome in COVID-19: a major mechanism of morbidity and mortality. Int. Rev. Immunol. *41*, 217–230. https://doi.org/10.1080/08830185.2021.1884248.
7. McGonagle, D., Sharif, K., O'Regan, A., and Bridgewood, C. (2020). The role of cytokines including interleukin-6 in COVID-19 induced pneumonia and macrophage activation syndrome-like disease. Autoimmun. Rev. *19*, 102537. https://doi.org/10.1016/j.autrev.2020.102537.
8. Mulchandani, R., Lyngdoh, T., and Kakkar, A.K. (2021). Deciphering the COVID-19 cytokine storm: systematic review and meta-analysis. Eur. J. Clin. Invest. *51*, e13429. https://doi.org/10.1111/eci.13429.
9. Liao, M., Liu, Y., Yuan, J., Wen, Y., Xu, G., Zhao, J., Cheng, L., Li, J., Wang, X., Wang, F., et al. (2020). Single-cell landscape of bronchoalveolar immune cells in patients with COVID-19. Nat. Med. *26*, 842–844. https://doi.org/10.1038/s41591-020-0901-9.
10. Silvin, A., Chapuis, N., Dunsmore, G., Goubet, A.-G., Dubuisson, A., Derosa, L., Almire, C., Hénon, C., Kosmider, O., Droin, N., et al. (2021). Elevated calprotectin and abnormal myeloid cell subsets discriminate

severe from mild COVID-19. Cell *182*. 1401–1418.e18. https://doi.org/10.1016/j.cell.2020.08.002.

11. Kyriazopoulou, E., Poulakou, G., Milionis, H., Metallidis, S., Adamis, G., Tsiakos, K., Fragkou, A., Rapti, A., Damoulari, C., Fantoni, M., et al. (2021). Early treatment of COVID-19 with anakinra guided by soluble urokinase plasminogen receptor plasma levels: a double-blind, randomized controlled phase 3 trial. Nat. Med. *27*, 1752–1760. https://doi.org/10.1038/s41591-021-01499-z.
12. Kyriazopoulou, E., Huet, T., Cavalli, G., Gori, A., Kyprianou, M., Pickkers, P., Eugen-Olsen, J., Clerici, M., Veas, F., Chatellier, G., et al. (2021). Effect of anakinra on mortality in patients with COVID-19: a systematic review and patient-level meta-analysis. Lancet Rheumatol. *3*, e690–e697. https://doi.org/10.1016/S2665-9913(21)00216-2.
13. REMAP-CAP Investigators, Gordon, A.C., Mouncey, P.R., Al-Beidh, F., Rowan, K.M., Nichol, A.D., Arabi, Y.M., Annane, D., Beane, A., Bentum-Puijk, W. van, et al. (2021). Interleukin-6 receptor antagonists in critically ill patients with Covid-19. N. Engl. J. Med. *384*, 1491–1502. https://doi.org/10.1056/NEJMoa2100433.
14. Broz, P., and Dixit, V.M. (2016). Inflammasomes: mechanism of assembly, regulation and signalling. Nat. Rev. Immunol. *16*, 407–420. https://doi.org/10.1038/nri.2016.58.
15. Chi, Y., Ge, Y., Wu, B., Zhang, W., Wu, T., Wen, T., Liu, J., Guo, X., Huang, C., Jiao, Y., et al. (2020). Serum cytokine and chemokine profile in relation to the severity of coronavirus disease 2019 in China. J. Infect. Dis. *222*, 746–754. https://doi.org/10.1093/infdis/jiaa363.
16. McElvaney, O.J., McEvoy, N.L., McElvaney, O.F., Carroll, T.P., Murphy, M.P., Dunlea, D.M., Ní Choileáin, O.N., Clarke, J., O'Connor, E., Hogan, G., et al. (2020). Characterization of the inflammatory response to severe COVID-19 illness. Am. J. Respir. Crit. Care Med. *202*, 812–821. https://doi.org/10.1164/rccm.202005-1583OC.
17. Alnefeesi, Y., Siegel, A., Lui, L.M.W., Teopiz, K.M., Ho, R.C.M., Lee, Y., Nasri, F., Gill, H., Lin, K., Cao, B., et al. (2020). Impact of SARS-CoV-2 infection on cognitive function: a systematic review. Front. Psychiatry *11*, 621773. https://doi.org/10.3389/fpsyt.2020.621773.
18. Kempuraj, D., Selvakumar, G.P., Ahmed, M.E., Raikwar, S.P., Thangavel, R., Khan, A., Zaheer, S.A., Iyer, S.S., Burton, C., James, D., and Zaheer, A. (2020). COVID-19, mast cells, cytokine storm, psychological stress, and neuroinflammation. Neuroscientist *26*, 402–414. https://doi.org/10.1177/1073858420941476.
19. Yap, J.K.Y., Moriyama, M., and Iwasaki, A. (2020). Inflammasomes and pyroptosis as therapeutic targets for COVID-19. J. Immunol. *205*, 307–312. https://doi.org/10.4049/jimmunol.2000513.
20. Allen, I.C., Scull, M.A., Moore, C.B., Holl, E.K., McElvania-TeKippe, E., Taxman, D.J., Guthrie, E.H., Pickles, R.J., and Ting, J.P.Y. (2009). The NLRP3 inflammasome mediates in vivo innate immunity to influenza A virus through recognition of viral RNA. Immunity *30*, 556–565. https://doi.org/10.1016/j.immuni.2009.02.005.
21. Thomas, P.G., Dash, P., Aldridge, J.R., Ellebedy, A.H., Reynolds, C., Funk, A.J., Martin, W.J., Lamkanfi, M., Webby, R.J., Boyd, K.L., et al. (2009). The intracellular sensor NLRP3 mediates key innate and healing responses to influenza A virus via the regulation of caspase-1. Immunity *30*, 566–575. https://doi.org/10.1016/j.immuni.2009.02.006.
22. Ichinohe, T., Lee, H.K., Ogura, Y., Flavell, R., and Iwasaki, A. (2009). Inflammasome recognition of influenza virus is essential for adaptive immune responses. J. Exp. Med. *206*, 79–87. https://doi.org/10.1084/jem.20081667.
23. Lupfer, C., Malik, A., and Kanneganti, T.-D. (2015). Inflammasome control of viral infection. Curr. Opin. Virol. *12*, 38–46. https://doi.org/10.1016/j.coviro.2015.02.007.
24. Swanson, K.V., Deng, M., and Ting, J.P.Y. (2019). The NLRP3 inflammasome: molecular activation and regulation to therapeutics. Nat. Rev. Immunol. *19*, 477–489. https://doi.org/10.1038/s41577-019-0165-0.
25. Fitzgerald, K.A., and Kagan, J.C. (2020). Toll-like receptors and the control of immunity. Cell *180*, 1044–1066. https://doi.org/10.1016/j.cell.2020.02.041.
26. Zheng, M., Karki, R., Williams, E.P., Yang, D., Fitzpatrick, E., Vogel, P., Jonsson, C.B., and Kanneganti, T.D. (2021). TLR2 senses the SARS-CoV-2 envelope protein to produce inflammatory cytokines. Nat. Immunol. *22*, 829–838. https://doi.org/10.1038/s41590-021-00937-x.
27. Ding, J., Wang, K., Liu, W., She, Y., Sun, Q., Shi, J., Sun, H., Wang, D.-C., and Shao, F. (2016). Pore-forming activity and structural autoinhibition of the gasdermin family. Nature *535*, 111–116. https://doi.org/10.1038/nature18590.
28. Kayagaki, N., Stowe, I.B., Lee, B.L., O'Rourke, K., Anderson, K., Warming, S., Cuellar, T., Haley, B., Roose-Girma, M., Phung, Q.T., et al. (2015). Caspase-11 cleaves gasdermin D for non-canonical inflammasome signalling. Nature *526*, 666–671. https://doi.org/10.1038/nature15541.
29. Liu, X., Zhang, Z., Ruan, J., Pan, Y., Magupalli, V.G., Wu, H., and Lieberman, J. (2016). Inflammasome-activated gasdermin D causes pyroptosis by forming membrane pores. Nature *535*, 153–158. https://doi.org/10.1038/nature18629.
30. Shi, J., Zhao, Y., Wang, K., Shi, X., Wang, Y., Huang, H., Zhuang, Y., Cai, T., Wang, F., and Shao, F. (2015). Cleavage of GSDMD by inflammatory caspases determines pyroptotic cell death. Nature *526*, 660–665. https://doi.org/10.1038/nature15514.
31. Ramos, I., and Fernandez-Sesma, A. (2012). Cell receptors for influenza A viruses and the innate immune response. Front. Microbiol. *3*, 117. https://doi.org/10.3389/fmicb.2012.00117.
32. Hoffmann, M., Kleine-Weber, H., Schroeder, S., Krüger, N., Herrler, T., Erichsen, S., Schiergens, T.S., Herrler, G., Wu, N.-H., Nitsche, A., et al. (2020). SARS-CoV-2 cell entry depends on ACE2 and TMPRSS2 and is blocked by a clinically proven protease inhibitor. Cell *181*. 271.e8–280.e8. https://doi.org/10.1016/j.cell.2020.02.052.
33. Lan, J., Ge, J., Yu, J., Shan, S., Zhou, H., Fan, S., Zhang, Q., Shi, X., Wang, Q., Zhang, L., and Wang, X. (2020). Structure of the SARS-CoV-2 spike receptor-binding domain bound to the ACE2 receptor. Nature *581*, 215–220. https://doi.org/10.1038/s41586-020-2180-5.
34. Rockx, B., Kuiken, T., Herfst, S., Bestebroer, T., Lamers, M.M., Oude Munnink, B.B.O., Meulder, D. de, Amerongen, G. van, Brand, J. van den, Okba, N.M.A., et al. (2020). Comparative pathogenesis of COVID-19, MERS, and SARS in a nonhuman primate model. Science *368*, 1012–1015. https://doi.org/10.1126/science.abb7314.
35. Sungnak, W., Huang, N., Bécavin, C., Berg, M., Queen, R., Litvinukova, M., Talavera-López, C., Maatz, H., Reichart, D., Sampaziotis, F., et al. (2020). SARS-CoV-2 entry factors are highly expressed in nasal epithelial cells together with innate immune genes. Nat. Med. *26*, 681–687. https://doi.org/10.1038/s41591-020-0868-6.
36. Zhao, Y., Zhao, Z., Wang, Y., Zhou, Y., Ma, Y., and Zuo, W. (2020). Single-cell RNA expression profiling of ACE2, the receptor of SARS-CoV-2. Am. J. Respir. Crit. Care Med. *202*, 756–759. https://doi.org/10.1164/rccm.202001-0179LE.
37. Ferreira, A.C., Soares, V.C., Azevedo-Quintanilha, I.G., Dias, S.da S.G., Fintelman-Rodrigues, N., Sacramento, C.Q., Mattos, M., Freitas, C.S., Temerozo, J.R., Teixeira, L., et al. (2021). SARS-CoV-2 engages inflammasome and pyroptosis in human primary monocytes. Cell Death Discov. *7*, 43. https://doi.org/10.1038/s41420-021-00428-w.
38. Rodrigues, T.S., Sá, K.S.G. de, Ishimoto, A.Y., Becerra, A., Oliveira, S., Almeida, L., Gonçalves, A.V., Perucello, D.B., Andrade, W.A., Castro, R., et al. (2021). Inflammasomes are activated in response to SARS-CoV-2 infection and are associated with COVID-19 severity in patients. J. Exp. Med. *218*, e20201707. https://doi.org/10.1084/jem.20201707.
39. Theobald, S.J., Simonis, A., Georgomanolis, T., Kreer, C., Zehner, M., Eisfeld, H.S., Albert, M.C., Chhen, J., Motameny, S., Erger, F., et al. (2021). Long-lived macrophage reprogramming drives spike protein-mediated inflammasome activation in COVID-19. EMBO Mol. Med. *13*, e14150. https://doi.org/10.15252/emmm.202114150.
40. Junqueira, C., Crespo, Â., Ranjbar, S., de Lacerda, L.B., Lewandrowski, M., Ingber, J., Parry, B., Ravid, S., Clark, S., Schrimpf, M.R., et al. (2022). FcγR-mediated SARS-CoV-2 infection of monocytes activates

inflammation. Nature *606*, 576–584. https://doi.org/10.1038/s41586-022-04702-4.

41. Sefik, E., Qu, R., Junqueira, C., Kaffe, E., Mirza, H., Zhao, J., Brewer, J.R., Han, A., Steach, H.R., Israelow, B., et al. (2022). Inflammasome activation in infected macrophages drives COVID-19 pathology. Nature *606*, 585–593. https://doi.org/10.1038/s41586-022-04802-1.

42. Hou, Y.J., Okuda, K., Edwards, C.E., Martinez, D.R., Asakura, T., Kenneth, H.D., 3rd, Kato, T., Lee, R.E., Yount, B.L., Mascenik, T.M., et al. (2020). SARS-CoV-2 reverse genetics reveals a variable infection gradient in the respiratory tract. Cell *182*. 429–446.e14. https://doi.org/10.1016/j.cell.2020.05.042.

43. Planès, R., Pinilla, M., Santoni, K., Hessel, A., Passemar, C., Lay, K., Paillette, P., Valadão, A.-L.C., Robinson, K.S., Bastard, P., et al. (2022). Human NLRP1 is a sensor of pathogenic coronavirus 3CL proteases in lung epithelial cells. Mol. Cell *82*. 2385–2400.e9. https://doi.org/10.1016/j.molcel.2022.04.033.

44. Chua, R.L., Lukassen, S., Trump, S., Hennig, B.P., Wendisch, D., Pott, F., Debnath, O., Thürmann, L., Kurth, F., Völker, M.T., et al. (2020). COVID-19 severity correlates with airway epithelium–immune cell interactions identified by single-cell analysis. Nat. Biotechnol. *38*, 970–979. https://doi.org/10.1038/s41587-020-0602-4.

45. Gaidt, M.M., Ebert, T.S., Chauhan, D., Ramshorn, K., Pinci, F., Zuber, S., O'Duill, F., Schmid-Burgk, J.L., Hoss, F., Buhmann, R., et al. (2017). The DNA inflammasome in human myeloid cells is initiated by a STING-cell death program upstream of NLRP3. Cell *171*. 1110–1124.e18. https://doi.org/10.1016/j.cell.2017.09.039.

46. Swanson, K.V., Junkins, R.D., Kurkjian, C.J., Holley-Guthrie, E., Pendse, A.A., El Morabiti, R.E., Petrucelli, A., Barber, G.N., Benedict, C.A., and Ting, J.P.Y. (2017). A noncanonical function of cGAMP in inflammasome priming and activation. J. Exp. Med. *214*, 3611–3626. https://doi.org/10.1084/jem.20171749.

47. Hornung, V., Ablasser, A., Charrel-Dennis, M., Bauernfeind, F., Horvath, G., Caffrey, D.R., Latz, E., and Fitzgerald, K.A. (2009). AIM2 recognizes cytosolic dsDNA and forms a caspase-1-activating inflammasome with ASC. Nature *458*, 514–518. https://doi.org/10.1038/nature07725.

48. Hare, D., Collins, S., Cuddington, B., and Mossman, K. (2016). The importance of physiologically relevant cell lines for studying virus–host interactions. Viruses *8*, 297. https://doi.org/10.3390/v8110297.

49. Fulcher, M.L., and Randell, S.H. (2012). Epithelial Cell Culture Protocols (Methods in Molecular Biology)*945*, Second Edition (Humana Press), pp. 109–121. https://doi.org/10.1007/978-1-62703-125-7_8.

50. Taabazuing, C.Y., Griswold, A.R., and Bachovchin, D.A. (2020). The NLRP1 and CARD8 inflammasomes. Immunol. Rev. *297*, 13–25. https://doi.org/10.1111/imr.12884.

51. Khan, S., Shafiei, M.S., Longoria, C., Schoggins, J.W., Savani, R.C., and Zaki, H. (2021). SARS-CoV-2 spike protein induces inflammation via TLR2-dependent activation of the NF-κB pathway. eLife *10*, e68563. https://doi.org/10.7554/eLife.68563.

52. Holness, C.L., and Simmons, D.L. (1993). Molecular cloning of CD68, a human macrophage marker related to lysosomal glycoproteins. Blood *81*, 1607–1613. https://doi.org/10.1182/blood.v81.6.1607.1607.

53. Aratani, Y. (2018). Myeloperoxidase: its role for host defense, inflammation, and neutrophil function. Arch. Biochem. Biophys. *640*, 47–52. https://doi.org/10.1016/j.abb.2018.01.004.

54. Robinson, K.S., Teo, D.E.T., Tan, K.S., Toh, G.A., Ong, H.H., Lim, C.K., Lay, K., Au, B.V., Lew, T.S., Chu, J.J.H., et al. (2020). Enteroviral 3C protease activates the human NLRP1 inflammasome in airway epithelia. Science *370*, 1–14. https://doi.org/10.1126/science.aay2002.

55. Zhong, F.L., Mamaï, O., Sborgi, L., Boussofara, L., Hopkins, R., Robinson, K., Szeverényi, I., Takeichi, T., Balaji, R., Lau, A., et al. (2016). Germline NLRP1 mutations cause skin inflammatory and cancer susceptibility syndromes via inflammasome activation. Cell *167*. 187.e17–202.e17. https://doi.org/10.1016/j.cell.2016.09.001.

56. Stutz, A., Horvath, G.L., Monks, B.G., and Latz, E. (2013). ASC speck formation as a readout for inflammasome activation. Methods Mol. Biol. *1040*, 91–101. https://doi.org/10.1007/978-1-62703-523-1_8.

57. Patel, V.I., and Metcalf, J.P. (2018). Airway macrophage and dendritic cell subsets in the resting human lung. Crit. Rev. Immunol. *38*, 303–331. https://doi.org/10.1615/CritRevImmunol.2018026459.

58. Wauters, E., Mol, P., Garg, A.D., Jansen, S., Herck, Y., Vanderbeke, L., Bassez, A., Boeckx, B., Malengier-Devlies, B., Timmerman, A., et al. (2021). Discriminating mild from critical COVID-19 by innate and adaptive immune single-cell profiling of bronchoalveolar lavages. Cell Res. *31*, 272–290. https://doi.org/10.1038/s41422-020-00455-9.

59. Bost, P., De Sanctis, F.D., Canè, S., Ugel, S., Donadello, K., Castellucci, M., Eyal, D., Fiore, A., Anselmi, C., Barouni, R.M., et al. (2021). Deciphering the state of immune silence in fatal COVID-19 patients. Nat. Commun. *12*, 1428. https://doi.org/10.1038/s41467-021-21702-6.

60. Mould, K.J., Moore, C.M., McManus, S.A., McCubbrey, A.L., McClendon, J.D., Griesmer, C.L., Henson, P.M., and Janssen, W.J. (2021). Airspace macrophages and monocytes exist in transcriptionally distinct subsets in healthy adults. Am. J. Respir. Crit. Care Med. *203*, 946–956. https://doi.org/10.1164/rccm.202005-1989OC.

61. He, J., Cai, S., Feng, H., Cai, B., Lin, L., Mai, Y., Fan, Y., Zhu, A., Huang, H., Shi, J., et al. (2020). Single-cell analysis reveals bronchoalveolar epithelial dysfunction in COVID-19 patients. Protein Cell *11*, 680–687. https://doi.org/10.1007/s13238-020-00752-4.

62. Schulte-Schrepping, J., Reusch, N., Paclik, D., Baßler, K., Schlickeiser, S., Zhang, B., Krämer, B., Krammer, T., Brumhard, S., Bonaguro, L., et al. (2020). Severe COVID-19 is marked by a dysregulated myeloid cell compartment. Cell *182*. 1419–1440.e23. https://doi.org/10.1016/j.cell.2020.08.001.

63. Tirosh, I., Izar, B., Prakadan, S.M., Wadsworth, M.H., Treacy, D., Trombetta, J.J., Rotem, A., Rodman, C., Lian, C., Murphy, G., et al. (2019). Dissecting the multicellular ecosystem of metastatic melanoma by single-cell RNA-seq. Science *352*, 189–196. https://doi.org/10.1126/science.aad0501.

64. Hao, Y., Hao, S., Andersen-Nissen, E., Mauck, W.M., 3rd, Zheng, S., Butler, A., Lee, M.J., Wilk, A.J., Darby, C., Zager, M., et al. (2021). Integrated analysis of multimodal single-cell data. Cell *184*. 3573–3587.e29. https://doi.org/10.1016/j.cell.2021.04.048.

65. Tanaka, T., Narazaki, M., and Kishimoto, T. (2014). IL-6 in inflammation, immunity, and disease. Cold Spring Harb. Perspect. Biol. *6*, a016295. https://doi.org/10.1101/cshperspect.a016295.

66. Abani, O., Abbas, A., Abbas, F., Abbas, M., Abbasi, S., Abbass, H., Abbott, A., Abdallah, N., Abdelaziz, A., and Abdelfattah, M. (2021). Tocilizumab in patients admitted to hospital with COVID-19 (RECOVERY): a randomised, controlled, open-label, platform trial. Lancet *397*, 1637–1645. https://doi.org/10.1016/S0140-6736(21)00676-0.

67. Zheng, J., Wang, Y., Li, K., Meyerholz, D.K., Allamargot, C., and Perlman, S. (2021). Severe acute respiratory syndrome coronavirus 2–induced immune activation and death of monocyte-derived human macrophages and dendritic cells. J. Infect. Dis. *223*, 785–795. https://doi.org/10.1093/infdis/jiaa753.

68. Lowery, S.A., Sariol, A., and Perlman, S. (2021). Innate immune and inflammatory responses to SARS-CoV-2: implications for COVID-19. Cell Host Microbe *29*, 1052–1062. https://doi.org/10.1016/j.chom.2021.05.004.

69. Bryce, C., Grimes, Z., Pujadas, E., Ahuja, S., Beasley, M.B., Albrecht, R., Hernandez, T., Stock, A., Zhao, Z., AlRasheed, M.R., et al. (2021). Pathophysiology of SARS-CoV-2: the Mount Sinai COVID-19 autopsy experience. Mod. Pathol. *34*, 1456–1467. https://doi.org/10.1038/s41379-021-00793-y.

70. Guo, H., and Ting, J.P.-Y. (2020). Inflammasome assays in vitro and in mouse models. Curr. Protoc. Immunol. *131*, e107. https://doi.org/10.1002/cpim.107.

71. Hafemeister, C., and Satija, R. (2019). Normalization and variance stabilization of single-cell RNA-seq data using regularized negative binomial

regression. Genome Biol. *20*, 296. https://doi.org/10.1186/s13059-019-1874-1.

72. Stuart, T., Butler, A., Hoffman, P., Hafemeister, C., Papalexi, E., Mauck, W.M., Hao, Y., Stoeckius, M., Smibert, P., and Satija, R. (2019). Comprehensive integration of single-cell data. Cell *177*. 1888–1902.e21. https://doi.org/10.1016/j.cell.2019.05.031.

73. Levine, J.H., Simonds, E.F., Bendall, S.C., Davis, K.L., Amir, el-A.D., Tadmor, M.D., Litvin, O., Fienberg, H.G., Jager, A., Zunder, E.R., et al. (2015). Data-driven phenotypic dissection of AML reveals progenitor-like cells that correlate with prognosis. Cell *162*, 184–197. https://doi.org/10.1016/j.cell.2015.05.047.

74. Okuda, K., Dang, H., Kobayashi, Y., Carraro, G., Nakano, S., Chen, G., Kato, T., Asakura, T., Gilmore, R.C., Morton, L.C., et al. (2021). Secretory cells dominate airway CFTR expression and function in human airway superficial epithelia. Am. J. Respir. Crit. Care Med. *203*, 1275–1289. https://doi.org/10.1164/rccm.202008-3198OC.

Please cite this article in press as: Barnett et al., An epithelial-immune circuit amplifies inflammasome and IL-6 responses to SARS-CoV-2, Cell Host & Microbe (2022), https://doi.org/10.1016/j.chom.2022.12.005

STAR★METHODS

KEY RESOURCES TABLE

REAGENT or RESOURCE	SOURCE	IDENTIFIER
Antibodies		
Rabbit Anti-ASC	Adipogen	RRID: AB_2885200
Goat Anti-Myeloperoxidase	R&D Systems	RRID: AB_2250866
Mouse Anti-human CD68	Agilent Dako	RRID: AB_2074844
Rabbit Anti-human CD68	Cell Signaling Technology	RRID: AB_2799882
Mouse Anti-ABCA3	Seven Hills Bioreagents	RRID: AB_577285
Mouse Anti-human CD11c	ThermoFisher	RRID: AB_2881379
Donkey anti-Rabbit IgG (H+L) Highly Cross-Adsorbed Secondary Antibody, Alexa Fluor 488	ThermoFisher	RRID: AB_2535792
Donkey anti-Goat IgG (H+L) Highly Cross-Adsorbed Secondary Antibody, Alexa Fluor 488	ThermoFisher	RRID: AB_2534102
Donkey anti-Mouse IgG (H+L) Highly Cross-Adsorbed Secondary Antibody, Alexa Fluor Plus 555	ThermoFisher	RRID: AB_2762848
Donkey anti-Rabbit IgG (H+L) Highly Cross-Adsorbed Secondary Antibody, Alexa Fluor Plus 647	ThermoFisher	RRID: AB_2762835
Donkey anti-Mouse IgG (H+L) Highly Cross-Adsorbed Secondary Antibody, Alexa Fluor Plus 647	ThermoFisher	RRID: AB_2762830
Bacterial and virus strains		
SARS-CoV-2 USA-WA1/2020	BEI Resources	NR52281
icSARS-CoV-2-WT	Hou et al.[42]	Genbank: MT461669
Biological samples		
Mouse serum anti-SARS-CoV-2 Spike	Hou et al.[42]	N/A
Human bronchial epithelial cells	Marsico Lung Institute, UNC	N/A
Human lung samples from previously healthy individuals unsuitable for transplant	Carolina Donor Services (Durham, NC), the National Disease Research Interchange (Philadelphia, PA), & the International Institute for Advancement of Medicine (Edison, NJ)	N/A
Human COVID-19 lung samples	Drs. Edana Stroberg (Office of the Chief Medical Examiner, Oklahoma City, OK) & Ross. E. Zumwalt (University of New Mexico, Albuquerque, NM)	N/A
Anonymous donor leukapheresis samples	Gulf Coast Blood	N/A
Chemicals, peptides, and recombinant proteins		
Pam3-CSK4	Invivogen	Cat# tlrl-pms
Poly(I:C) HMW	Invivogen	Cat# tlrl-pic
Nigericin	Invivogen	Cat# tlrl-nig
ATP	Invivogen	Cat# tlrl-atpl
Poly(dA:dT)	Invivogen	Cat# tlrl-patn
Flagellin (recombinant, purified)	Gift from Dr. Ed Miao	N/A
Bay11-7082	Invivogen	Cat# tlrl-b82
Chloroquine	Invivogen	Cat# tlrl-chq
VX-765	Invivogen	Cat# inh-vx765i-1
C29	MedChem Express	Cat# HY-100461

(*Continued on next page*)

Please cite this article in press as: Barnett et al., An epithelial-immune circuit amplifies inflammasome and IL-6 responses to SARS-CoV-2, Cell Host & Microbe (2022), https://doi.org/10.1016/j.chom.2022.12.005

Continued

REAGENT or RESOURCE	SOURCE	IDENTIFIER
MMG-11	Tocris	Cat# 6858
H151	Invivogen	Cat# inh-h151
MCC950	Invivogen	Cat# inh-mcc
Benzonase® Nuclease	Millipore Sigma	Cat# 70664-3
Recombinant human IL-1β	Peprotech	Cat# 200-01B
Recombinant SARS-CoV-2 E Protein (Avi Epitope Tag) His (N-term) Avi-tag Protein	Novus	Cat#NBP2-90986
Recombinant SARS-CoV-2 S Protein	R&D Systems	Cat# 10639-CV-100
Critical commercial assays		
Ficoll-Paque™	Sigma	Cat#GE17-1440-02
TRIzol™	ThermoFisher	Cat#15596026
Direct-zol RNA Miniprep	ZYMO Research	Cat#R2052
iScript™ cDNA Synthesis Kit	Bio-Rad	Cat# 1708890
iTaq™ Universal SYBR Green Supermix	Bio-Rad	Cat# 17125120
RNAScope Multiplex Flourescent Reagent Kit V2	ACD Bio	Cat#323100
RNAScope 2.5 HD Reagent Kit-RED	ACD Bio	Cat#322430
RNAScope Probe *NLRP1* (channel 1)	ACD Bio	Cat# 436859
RNAScope Probe *NLRP3* (channel 1)	ACD Bio	Cat# 478021
RNAScope Probe *AIM2* (channel 1)	ACD Bio	Cat# 577931
RNAScope Probe *CASP1* (channel 1)	ACD Bio	Cat# 417631
RNAScope Probe *ABCA3* (channel 3)	ACD Bio	Cat# 555501-C3
RNAScope Probe *MPO* (channel 3)	ACD Bio	Cat# 603091-C3
RNAScope Probe *CD68* (channel 2)	ACD Bio	Cat# 560591-C2
RNAScope Probe *IL1B* (channel 2)	ACD Bio	Cat# 310361-C2
RNAScope Probe *IL6* (channel 1)	ACD Bio	Cat# 310371
Vector® TrueVIEW® Autofluorescence Quenching Kit	Vector Laboratories	Cat# SP-8400-15
VECTASHIELD Vibrance® Antifade Mounting Medium with DAPI	Vector Laboratories	Cat# H-1800
Roche Cell Cytotoxicity Kit (LDH)	Sigma	Cat#11644793001
QIAamp MinElute ccfDNA Mini Kit (50)	Qiagen	Cat# 55204
MyTaq™ HS Red Mix	Meridian Bioscience	Cat# BIO-25048
Human IL-1β ELISA Set II	BD Biosciences	Cat# 557953
Human Total IL-18/IL-1F4 Quantikine ELISA Kit	R&D Systems	Cat# DL180
ELISA MAX™ Deluxe Set Human IL-6	Biolegend	Cat#430515
Deposited data		
Single-cell landscape of bronchoalveolar immune cells in COVID-19 patients	Liao et al.[9]	GEO: GSE145926
Single-cell RNA sequencing of bronchoalveolar lavages from COVID-19 patients	Wauters et al.[58]	EGA: EGAS00001004717
Deciphering the state of immune silence in fatal COVID-19 patients	Bost et al.[59]	GEO: GSE157344
Single-cell sequencing of BALF reveals immune response of COV2019 infection	He et al.[61]	GEO: GSE147143
Bronchoalveolar lavage of healthy human adults	Mould et al.[60]	GEO: GSE151928
Original Code for scRNAseq analysis	This study	https://github.com/yuyingxie/An-epithelial-immune-circuit-amplifies-inflammasome-and-IL-6-responses-to-SARS-CoV-2

(*Continued on next page*)

Please cite this article in press as: Barnett et al., An epithelial-immune circuit amplifies inflammasome and IL-6 responses to SARS-CoV-2, Cell Host & Microbe (2022), https://doi.org/10.1016/j.chom.2022.12.005

Continued

REAGENT or RESOURCE	SOURCE	IDENTIFIER
Experimental models: Cell lines		
Vero-E6	ATCC	Cat# CRL-1586
Oligonucleotides		
See Table S1	This paper	N/A
Software and algorithms		
GraphPad Prism 9	GraphPad	https://graphpad.com
Zen Black	Zeiss	https://www.zeiss.com/microscopy/us/products/microscope-software.html
FIJI	Image J	https://fiji.sc/
Olyvia V3.1.1	Olympus	https://olympus-lifescience.com
Applied Biosystems QuantStudio V1.7.2	Applied Biosystems	https://www.thermofisher.com/us/en/home/global/forms/life-science/quantstudio-6-7-flex-software.html
R V4.0.2	R Project	https://cran.r-project.org/bin/windows/base/

RESOURCE AVAILABILITY

Lead contact

Further information and requests for resources and reagents should be directed to and will be fulfilled by the lead contact, Jenny P.-Y. Ting (jenny_ting@med.unc.edu).

Materials availability

This study did not generate new unique reagents.

Data and code availability

- This paper analyzes existing, publicly available data. The accession numbers for the datasets are listed in the key resources table.
- All original code is deposited at GitHub and is publicly available. DOIs are listed in the key resources table.
- Any additional information required to reanalyze the data reported in this paper is available from the lead contact upon request.

EXPERIMENTAL MODEL AND SUBJECT DETAILS

Human subjects

Human lungs from donors with no preexisting pulmonary disease that were unsuitable for transplantation were obtained from the University of North Carolina (UNC) Tissue Procurement and Cell Culture Core (institutional review board (IRB)-approved protocol #03-1396). Excised tissue specimens were dissected and fixed in 10% neutral buffered formalin for 48 hours followed by paraffin-embedding. Tissue blocks obtained from four COVID-19 autopsy lungs were obtained from Drs. Edana Stroberg (Office of the Chief Medical Examiner, Oklahoma City, OK), Ross. E. Zumwalt (University of New Mexico, Albuquerque, NM), and Leigh B. Thorne (University of North Carolina at Chapel Hill, Chapel Hill, NC). The paraffin blocks were cut to produce 5 μm serial sections for RNA *in situ* hybridization (RNA-ISH) and immunohistochemistry. Donor demographics are described as follows.

Donor 1

40-year-old male. Medical history: Diabetes mellitus. Clinical course: This donor had upper respiratory infection (URI) symptoms three days before he was found dead at home. No intubation occurred. Postmortem testing of the lung was positive for SARS-CoV-2.

Donor 2

91-year-old female. Medical history: coronary artery disease, hyperlipidemia, and hypertension. Clinical course: This donor was transferred to the ER because of URI symptoms, hypoxia, weakness, and shortness of breath. A nasal swab was positive for SARS-CoV-2. She was treated with high flow nasal canula but died from acute pneumonia due to SARS-CoV-2 complicated by an acute respiratory failure.

Donor 3

77-year-old male. Medical history: Acute pancreatitis, acute cholecystitis, and splenectomy. Clinical course: This donor was transferred to the ER because of fever and respiratory distress six days before death. He died shortly after arrival. A swab from the nasal cavity and the postmortem lung were positive for SARS-CoV-2.

Please cite this article in press as: Barnett et al., An epithelial-immune circuit amplifies inflammasome and IL-6 responses to SARS-CoV-2, Cell Host & Microbe (2022), https://doi.org/10.1016/j.chom.2022.12.005

Donor 4

42-year-old male. Medical history: Myotonic dystrophy, diabetes mellitus, hyperlipidemia, gastroesophageal reflux, cognitive deficits, dysarthria, and frequent falls. Clinical course: This donor was transferred to the ER because of cough and shortness of breath. He died shortly after arrival. No intubation occurred. SARS-CoV-2 was positive in nasopharyngeal swab, but negative in the postmortem lung.

Donor 5

No available clinical information.

Primary cell isolation and culture

Primary bronchial HAE were isolated and expanded as previously described.[49] Briefly, human bronchial epithelial cells were isolated from previously normal human lungs obtained from anonymous organ donors with lungs unsuitable for transplantation under UNC IRB-approved protocol (#03-1396). In brief, at two-passages post-isolation from human lungs, cells were plated onto 12mm 0.4μm polyester Transwell supports (Corning) coated with human placental collagen type IV (Sigma). Cells were maintained in UNC ALI media[49] at 37°C in 5% CO_2. Once cells were fully confluent, media from the apical chamber was removed, and cells were maintained at ALI and allowed to differentiate for 28 days after seeding. Media in the basolateral compartment was changed 3x/week. Well-differentiated HAE ALI cultures were utilized for experiments at 28-90 days after seeding.

Primary human PBMCs from anonymous donors (Gulf Coast Blood) were isolated from leukapheresis samples using a Ficoll-Paque™ density gradient (Sigma), frozen, and immediately used in experiments upon thawing. PBMCs were maintained in RPMI-1640 (Thermo) supplemented with 10% fetal bovine serum (FBS), 100 U/mL penicillin-streptomycin, L-glutamine, sodium pyruvate, and non-essential amino acids. Cells were maintained in an incubator at 37°C in 5% CO_2. For studies involving PBMCs with or without co-culture with Vero-E6 cells, PBMCs were maintained in MEM (Thermo) with 2% fetal bovine serum (FBS), 100 U/mL penicillin-streptomycin, L-glutamine, sodium pyruvate, and non-essential amino acids.

Vero cell line culture

Vero-E6 were maintained in MEM supplemented with 10% (maintenance media) or 2% (infection media) fetal bovine serum (FBS), 100 U/mL penicillin-streptomycin, L-glutamine, sodium pyruvate, and non-essential amino acids. For passage, confluent cells were rinsed with phosphate buffered saline (PBS), lifted with 0.25% trypsin, and plated at a 1:10 dilution factor. Cells were maintained in an incubator at 37°C in 5% CO_2.

METHOD DETAILS

Inflammasome stimulation

Inflammasome stimulation was performed using previously established protocols.[70] Briefly, cells were primed both basolateral and apical application of TLR ligands in ALI media 10μg/mL Pam3-CSK4 (Invivogen) or 0.5μg/mL Poly(I:C) (Invivogen). All apical ALI stimulations were delivered in a small volume of ALI media (75μL) to allow for continued air contact. After 3 hours, priming signals were removed, and inflammasome stimuli were added to the cultures. To activate the NLRP3 inflammasome, 40μM Nigericin (Invivogen) in ALI media was added to HAE culture apical and basolateral chambers for 1 hour. To activate the NLRP1/CARD8 inflammasome, 10μM Val-boroPro (R&D) was added to HAE culture apical and basolateral chambers for 18 hours. To activate the AIM2 inflammasome, poly(dA:dT) (Invivogen) was transfected into HAE cultures apically using Lipofectamine 2000 (Thermo) in Opti-MEM media (Thermo) and stimulated for 3 hours. To activate the NLRC4 inflammasome, purified flagellin (a generous gift from Dr. Ed Miao) was transfected into HAE cultures apically using DOTAP (Sigma) in Opti-MEM media and stimulated for 2 hours. To maximize transfection efficiency of p(dA:dT) and flagellin, the epithelial barrier was disrupted immediately prior to transfection by apical treatment with 30mM sodium caprate (Sigma) for 5 minutes at 37°C 5% CO_2. For NLRP3 inflammasome activation in human PBMCs, cells were primed with 1μg/mL Pam3-CSK4 (Invivogen) for 3 hours and then stimulated with 40μM Nigericin or 5mM ATP for 1 hour. For experiments looking at SARS-CoV-2 protein stimulation or SARS-CoV-2 infection in combination with known inflammasome stimulation, these treatments were applied as described in the text, preceded or followed by stimulations described above.

Following inflammasome activation, supernatants were collected and immediately frozen to measure IL-1β or IL-18 secretion by ELISA (BD OptEIA IL-1β or R&D IL-18) or LDH release (Roche/Sigma Cytotoxicity Detection Kit (LDH)). To collect apical supernatants from HAE ALI cultures, the apical surface was incubated with 250μL PBS for 30 minutes at 37°C 5% CO_2, gently mixed and removed, and then frozen until analysis by ELISA. ELISA values from apical wash samples (250μL) were normalized to the volume of basolateral media (1mL) to allow for direct comparison between the compartments. In some instances, these supernatants were pooled.

IL-1β or Protein/Ligand stimulation

Human PBMCs were treated in suspension in culture medium with recombinant human IL-1β (100pg/mL or 1ng/mL) or a vehicle control for indicated timepoints. Similarly, human PBMCs were treated in suspension in culture medium with recombinant SARS-CoV-2 E protein (1μg/mL), S protein trimer (1μg/mL) or Pam3-CSK4 (1μg/mL). HAE cultures were stimulated at the apical surface and in the basolateral compartment with recombinant human IL-1β (100pg/mL or 1ng/mL), Pam3-CSK4 (1μg/mL), or a vehicle control for indicated timepoints. Following treatment, cells were lysed in Trizol reagent for RNA isolation and subsequent RT-qPCR analysis. Cell

supernatants were collected and frozen until assessed by ELISA (Biolegend ELISA MAX™ human IL-6). Washes from the apical surface were collected as described above, stored frozen, and analyzed by ELISA.

Viral infections

SARS-CoV-2 USA-WA1/2020 or the synthetic clone of this strain icSARS-CoV-2 WT[42] were both utilized in these experiments due to the need to utilize two collaborating BSL3 facilities because of scheduling difficulties. HAE ALI cultures were rinsed twice with PBS for 30 minutes at 37°C to remove mucus prior to infection. Cells were infected apically with viral stocks diluted in PBS for 2 hours at 37°C in 5% CO_2 with frequent agitation, as described previously.[42] Following infection, cells were washed 3x with PBS for 5 minutes and kept at an ALI for the duration of the experiment at 37°C in 5% CO_2. Infection of PBMCs or Vero cell lines with SARS-CoV-2 occurred as described above with a few key differences. To infect PBMCs or Vero cell lines, culture media was removed and cells were incubated with diluted viral stocks in infection media (complete MEM 2%FBS, as described above) for 1 hour at 37°C in 5% CO_2 with frequent agitation. Following the infection period, inoculum was removed and wells were given fresh infection media for the experiment duration. WT SARS-CoV-2 stocks were propagated in Vero-E6 cells. All SARS-CoV-2 infections, propagation, and assays requiring samples with live virus (ELISA, plaque assay) were performed under biosafety level 3 (BSL-3) containment at negative pressure and in Tyvek suits with personal respirators.

Following infection, HAE ALI apical wash and basolateral supernatants were collected and frozen for analysis, as described above. For PBMCs, cells were pelleted at 500xg for 5 minutes, supernatants were frozen and collected for analysis by ELISA. Cell lysates were collected in TRIzol reagent (Thermo) for measurement of gene expression by reverse transcription quantitative PCR (RT-qPCR).

RT-qPCR

Following lysis in TRIzol reagent, RNA was isolated according to the manufacturer's protocol. RNA was converted into cDNA through reverse transcription using the iScript™ cDNA Synthesis Kit (Bio-Rad). Relative mRNA and viral RNA expression was then measured using the iTaq Universal SYBR Green Mastermix (Bio-Rad) on the Quantstudio 6 Real Time PCR System (Applied Biosystems). Primers used are listed in the key resources table.

PCR detection of DNA in supernatants

HAE supernatants were heat inactivated for 60 minutes and 60°C for removal from BSL3, dsDNA was isolated from these supernatants through spin column purification (Qiagen QIAamp MinElute ccfDNA Mini Kit), and then PCR amplification of genomic or mitochondrial DNA amplicons was performed (Meridian Bioscience MyTaq™ HS Red Mix). Cycle conditions are as follows: Denaure: 15s 98°C, Anneal: 15s 55°C, and Extend: 30s 72°C for 25 cycles followed by 5 minute extension period. Amplified dsDNA products were visualized on an agarose gel using SYBR green dye and analyzed in FIJI. Primers used are listed in the key resources table.

Plaque assay

Confluent Vero-E6 cells were infected with ten-fold serial dilutions of cell culture supernatants (PBMC/Vero) or apical washes (HAE cultures) to measure viral titer. Diluted samples were assayed in duplicate. Infections were performed for one hour as described above with frequent agitation. After 1 hour, overlay (1.25% carboxy methylcellulose and 1x alpha-MEM) was placed over the infected cells. Four days post infection, wells were fixed by adding 4% paraformaldehyde or formalin to each well. The overlay/fixative solution was removed, plates were submerged in fixative, rinsed with water and then stained for a minimum of 10 minutes with.25% crystal violet in water. Excess stain was removed, plates rinsed, and plaques were enumerated.

Integrated scRNA-seq meta-analysis

We retrieved single-cell RNA-Seq data from the following published datasets: GEO: GSE145926,[9] GEO: GSE147143,[61] GEO: GSE157344,[59] GEO: GSE151928,[60] and EGA: EGAS00001004717.[58] Collectively, 26 patients with severe COVID-19 disease, 5 patients with moderate or mild symptoms, and 3 healthy controls were included in the initial analysis, while 10 healthy donors and 24 severe patients were added in the projected data. In total, cells from 13 healthy donors, 5 mild/moderate patients, and 50 severe patients were analyzed. We only kept high-quality cells that had unique feature counts between 200 and 10,000 and mitochondrial reads of less than 20%. Cells with unique molecular identifiers counts below 500 were filtered out. After processing, a total of 117,497 high-quality transcriptomes of PBMCs were available for integration. We implemented the sctransform algorithm for the integrated data set using Seurat v.3 to normalize and remove the library size effect.[71] Then, we utilized the Mutual Nearest Neighbors algorithm to remove the batch effect between studies and between patients.[72] To concentrate biology signals, we selected the top 2,000 genes with the highest cell-to-cell variation, in conjunction with a set of immune cell subsets signature genes to stabilize the lineage segregation. These additional anchor features include *CXCR5*, *CD69*, *AIM2*, *IRF5*, *IRF1*, *IRF3*, *LGALS9*, *LY6E*, *NOS2*, *IL6*, *TNF*, *ISG15*, *GSDMD*, *CD8A*, *CD40*, *CD80*, *CD86*, *IL10*, *TGFB1*, *TMEM173*, *CD274*, *CXCL9*, *MRC1*, *SIGLEC15*, *TRDC*, *CD2*, *TRAC*, *CD4*, *CD8B*, *FOXP3*, *TRBC1*, *TRBC2*, *GZMB*, *EOMES*, *ICOS*, *CD3G*, *CD3E*, *IFNG*, *NCR1*, *CD19*, *CD79A*, *CD79B*, *ITGAM*, *ITGAX*, *BATF3*, *XCR1*, *GATA3*, *CTLA4*, *RORC*, *IL17A*, *BCL6*, *HAVCR2*, *TNFRSF4*, *TIGIT*, *CXCL10*, *MX1*, *IFNB1*, *IL3RA*, *NRP1*, *CLEC4C*, *FCER1A*, *TBX21*, *LAG3*, *IFNL3*, *PDCD1*, *CD14*, and *CD33*. We obtained the top 50 principal components (PCs) from the integrated data. Then, we employed the Shared Nearest Neighbor method to group cells, informing 22 distinct clusters with a resolution of 0.8.[73]

Please cite this article in press as: Barnett et al., An epithelial-immune circuit amplifies inflammasome and IL-6 responses to SARS-CoV-2, Cell Host & Microbe (2022), https://doi.org/10.1016/j.chom.2022.12.005

Immunohistochemistry

Immunohistochemical staining was performed on non-disease explant lung (control) and COVID-19 autopsy lung sections, according to previously described protocols.[42] Briefly, paraffin-embedded sections were baked at 60 °C for 2–4 hours and deparaffinized with xylene (2 changes × 10 min) and graded ethanol (100% 2 × 5 min, 95% 1 × 5 min, 70% 1 × 5 min). After rehydration, antigen retrieval was performed by boiling the slides in 0.1 M sodium citrate pH 6.0 (3 cycles with microwave settings: 100% power for 6.5 min, 60% for 6 min, and 60% for 6 min, refilling the Coplin jars with distilled water after each cycle). After cooling and rinsing with distilled water, slides were washed in PBS and blocked with 4% normal donkey serum for one hour at RT. Primary antibodies (ASC:1:500, MPO: 1:200, CD68: 1:100, CD11c: 1:500, Anti-SARS mouse antiserum: 1:4000) were diluted in 4% normal donkey serum in PBST (phosphate-buffered saline containing 0.1% Triton X-100) and incubated overnight at 4 °C. Sections were washed in PBST, and secondary antibodies (Alexa Fluor 488 donkey anti-rabbit IgG, at 1:1000 dilution; Alexa Fluor 647 donkey anti-mouse IgG, at 1:1000 dilution and Alexa Fluor 750 donkey anti-goat IgG, at 1:1000 dilution) were applied for 60 min at RT. After washing in PBST, the Vector® TrueVIEW Autofluorescence Quenching Kit (Vector laboratories) was used to reduce background staining, and glass coverslips were placed over tissue sections with the VECTASHIELD® Vibrance™ Antifade Mounting Medium with DAPI (Vector laboratories). Cover slipped slides were scanned and digitized using an Olympus VS200 with a 20X 0.75 NA objective. Representative images were generated from these digitized composite images using Olyvia software or captured on a Zeiss LSM 710 inverted laser scanning confocal microscope with a 40X/1.4 Oil Plan Apo objective using Zen software.

RNA *in situ* hybridization (RNA-ISH)

RNA-ISH was performed on paraffin-embedded 5μm tissue sections of control and COVID-19 autopsy lung sections using the RNAscope 2.5 HD Reagent Kit-RED (chromogenic images) and Multiplex Fluorescent Assay Kit v2 (fluorescent images) according to the manufacturer's instructions (Advanced Cell Diagnostics). Sections were deparaffinized with xylene (2 changes × 5 min) and 100% ethanol (2 changes × 1 min), incubated with hydrogen peroxide for 10 min followed by target retrieval in boiling water for 15 min, and incubation with Protease Plus (Advanced Cell Diagnostics) for 15 min at 40°C. Slides were hybridized with custom probes at 40 °C for 2 hours, and signals were amplified according to the manufacturer's instructions. Cover slipped slides were scanned and digitized using an Olympus VS200 with a 20X 0.75 NA objective. Representative images were generated from these digitized composite images using Olyvia software or captured on a Zeiss LSM 710 inverted laser scanning confocal microscope with a 40X/1.4 Oil Plan Apo objective using Zen software.

QUANTIFICATION AND STATISTICAL ANALYSIS

Image quantification

Stained areas of *CASP1*, *NLRP1*, *NLRP3*, and *AIM2* mRNAs by chromogenic RNA-ISH in the alveolar regions were quantitated using FIJI software as previously described.[74] Briefly, alveolar regions were cropped from the field, and staining of each mRNA was converted to a gray-scale image. Optimized threshold value was determined by adjusting the threshold to accurately represent the original images. We applied the optimized threshold value to all the sections. The stained-areas were normalized to alveolar areas. Fluorescent staining of lung samples was counted manually from randomly selected fields of view with an $n \geq 500$ for each biological replicate. ASC speck frequency was normalized to the frequency of nuclei, as indicated by DAPI staining. Co-incidence of ASC specks with other markers was normalized to the total number of nuclei-associated ASC specks, as indicated by DAPI staining. Co-incidence of genes with other markers was normalized to the total number of gene-associated nuclei, as indicated by DAPI staining.

Statistical analysis

With the exception of scRNAseq data, all statistical analysis was performed using Graphpad Prism 8 software. All experiments were performed in triplicate and represent 3 independent biological replicates. For comparisons in which multiple variables were tested with multiple conditions, two-way ANOVA analysis with Tukey's, Dunnet's or Sidak's multiple comparison test correction was performed, as indicated in figure legends. For multiple comparisons of groups with a single independent variable, one-way ANOVA analysis with Tukey's or Dunnet's multiple comparison test correction was performed, as indicated in figure legends. Unpaired two-tailed t tests were used to compare two groups. Asterisk coding is as follows: * p<= 0.05; ** p<=0.01; *** p<=0.001; **** p<=0.0001. Data with error bars depict the average with the SEM.

scRNAseq Statistical analysis

Cell type differential abundance analyses were performed using the R package *ALDEx2*, which utilize centered log-ratio transformation to ensure the data to be scale invariant and sub-compositionally coherent. To test the significance of Inflammasome score and gene expression quantile across disease statuses, we employed a linear quantile mixed model via the R package *lqmm*, where patient IDs were treated as a random effect. To enhance the rigor of the model, we removed samples that only had fewer than 5 cells in the given clusters. To test the significance of Inflammasome score and inflammasome genes on pool cells among disease status, we performed the non-parametric Kruskal-Wallis test taking account the fact that the data distributions are not Gaussian. Post-hoc Dunn's tests were conducted to determine pair-wise differences between disease status.